공학박사 학위논문

Fabrication and characterization of solution-processed polymer light-emitting diodes

용액 공정 고분자 발광 다이오드의 제작 및 소자 특성 평가

2013 년 2 월

서울대학교 대학원

공과대학 전기컴퓨터공학부

양 정 진

Fabrication and characterization of solution-processed polymer light-emitting diodes

지도교수 이 창 희

이 논문을 공학박사 학위논문으로 제출함

2013 년 2 월

서울대학교 대학원

공과대학 전기컴퓨터공학부

양 정 진

양정진의 박사 학위논문을 인준함

2013 년 1 월

위 원 장	황 기 웅	(인)
부위원장	이 창 희	(인)
위 원	홍 용 택	(인)
위 원	진 병 두	(인)
위 원	곽 정 훈	(인)

Abstract

Fabrication and characterization of solution-processed polymer light-emitting diodes

Jungjin Yang

School of Electrical Engineering and Computer Science

The Graduate School

Seoul National University

Organic light-emitting diodes (OLEDs) have received much attention due to their great potentials as flat panel displays and solid-state lighting. OLEDs can be fabricated using either vacuum evaporation or solution process; the latter method is considered more favorable from a higher throughput and low cost fabrication. Many research groups have developed their efforts on the solution -processed OLEDs and significant improvements have been reported. However, despite all these successes, there is almost no attempt to fabricate all solution-processed OLEDs. This thesis discusses the fabrication and characterization of solution-processed polymer light-emitting diodes (PLEDs) and finally all solution-processed PLEDs.

In a conventional device structure, we demonstrate solution-processed KBH_4 doped 3TPYMB layer as n-type doped electron transport layer and

introduce this layer in the fabrication of high efficiency PLEDs. Furthermore, we fabricate PLEDs with two conjugated polyelectrolyte materials of PEO and PFN-P1; these devices show high performance. In case of PLEDs with KBH_4 doped 3TPYMB layer and PFN-P1 layer, the devices work successfully with Liq/Al bilayer cathode as well as with Ag electrode. We fabricate all solution-processed PLEDs with such efficient layers and ink-jet printed Ag electrode, but those layers are diluted by Ag ink solvent and device fabrication is impossible. Due to this problem, all solution-processed PLEDs are fabricated by the following processes; Ag is printed on poly(dimethylsiloxane) (PDMS) and it is transplanted onto pre-fabricated PLEDs without cathode.

We also develop solution-processed PLEDs with an inverted device structure. For improving an electron injection, self-assembled monolayer (SAM) is applied to ZnO layer. Because the effect of SAM is low, inverted PLEDs with PFN-P1 layer are fabricated. For introducing solution-processed hole injection layer, FSO-100 doped PEDOT:PSS, MoO_3 nanoparticles and sol-gel V_2O_5 are used; PLEDs with sol-gel V_2O_5 show best performances above all. Finally, we fabricate all solution-processed inverted PLEDs with sol-gel V_2O_5 and direct ink-jet printed Ag. We think that the fabrication methods and device structures developed in this thesis are helpful for developing high efficiency all solution-processed OLEDs.

Keywords: solution process, polymer light-emitting diodes, n-doping, conjugated polyelectrolyte, ink-jet printing

Student Number: 2007-21014

Contents

List of Tables

List of Figures

Chapter 1. Introduction

1.1 Organic Light-Emitting Diodes

Recently, Organic light-emitting diodes (OLEDs) are emerging as a leading next generation technology for display industry and becoming a strong competitor for the liquid crystal display (LCD) technology. Displays based on OLEDs have many advantages such as brilliant colors, high contrast levels, large viewing angles, high efficiencies, and potentials for a low-cost fabrication. The OLED display already entered the commercial market. It has been used in mobile phones of many manufacturers (Samsung, HTC, Nokia, etc.) and Samsung introduced the first 55 inch OLED television at CES 2012 as shown in Figure 1.1. Besides, many display manufacturers such as LG, Sony, and Panasonic announced a mass production of OLED television.

Figure 1.1 The first 55 inch OLED television introduced by Samsung at CES 2012.

The first electroluminescence (EL) in organic devices was reported by Pope and coworkers in 1963 [1]. They observed EL from a single crystal of anthracene being sandwiched in between electrodes when the applied voltage reached about 400 V. However, the crystals were 10–20 μm and it is difficult to apply in practical applications. Subsequently, Vicett and coworkers fabricated light-emitting diodes with vacuum evaporation of polycrystalline anthracene thin films [2]. Though the voltage required to generate light is significantly reduced, electron-hole combination occurred very close to the injecting contact and the external quantum efficiency (EQE) was limited to less than 0.1%.

The OLEDs were not appropriate for practical applications until the first bilayer OLED by Tang and VanSlyke in 1987 [3]. They showed a green emitting OLED with high luminance more than 1000 cd/m^2 as well as EQE about 1% at a low bias of 10 V. The use of hetero-structure, consisting of aromatic diamine as the hole transporting layer (HTL) and 8-hydroxyquinoline aluminum (Alq_3) as the electron transporting layer (ETL), not only improved the transporting performance but also moved the recombination zone well away from electrodes to obtain high efficiency. Later in 1989, Tang and coworkers improved the device efficiency by two times by introducing doping systems [4]. This device separates the charge transport from the light emitting, thus allowing individually tuning of material properties. The EQE of their red emitting devices was about 2%.

Following the advancement of OLEDs based on small molecules, in 1990 Burroughes *et al.* successfully demonstrated the first polymer light-

emitting diodes (PLEDs) with conjugated polymer of poly(p-phenylene vinylene) (PPV) [5]. In this device, PPV thin films prepared by spin-coating a precursor polymer for light-emitting element, high work function oxide (indium oxide) as the anode was used and low work function metal (Al) by a thermal evaporation was used as the cathode. In contrast with devices by vacuum evaporation systems of small molecules, the quantum efficiency of the PLED was low about 0.05%. However, one of the outstanding features employed in this device is that solution processes have potential advantages of the simple fabrication in comparison with vacuum evaporations.

After this, a large number of studies to improve the performance of OLEDs have been conducted. The significant improvement in device performance was the demonstration of the phosphorescent OLEDs using phosphorescent materials by Baldo *et al.* in 1998 [6]. They enhanced the efficiency of OLEDs by introducing the phosphorescent dye 2,3,7,8,12,13,17,18-octaethyl-21H,23H-porphine platinum(II) (PtOEP). A maximum internal quantum efficiency of OLEDs with the fluorescent materials is limited to 25% because the singlet and triplet excited states are generated with the ratio of 1:3. For phosphorescent materials, the radiative recombination of all excitons allowed by introducing heavy metal atoms such as platinum (^{78}Pt) or iridium (^{77}Ir) into organic molecules. The use of phosphorescent emitters of heavy-metal complexes such as PtOEP [6] or fac-tris(2-phenypyridine) iridium ($Ir(ppy)_3$) [7] enabled 100% of internal quantum efficiency [8]. So far, a number of OLED materials have been successfully developed.

However, a large portion of emitting light in OLEDs is still wasted due to optical losses by a glass substrate, indium-tin-oxide (ITO) electrode, and several organic layers. Only 20–30% of the emitted light can be escaped to air in OLEDs. Recently, many researchers have studied to increase outcoupling efficiency by using various methods such as microlens array [9], substrate surface texturing [10], scattering film [11], low index grid [12] and high index substrate [13].

Despite these improvements, the commercial developments of OLEDs such as flat panel displays (FPDs) or solid-state lightings ware retarded by some problems. While red and green OLED emitters have long lifetimes over 100,000 hours, the blue component shows relatively short lifetime about 20,000 hours for phosphorescent and about 10,000 hours for fluorescent emitters. The differential aging of three element colors will cause a color shift in these devices, which is a severe limit to many applications of OLEDs.

1.2 Solution-processed PLEDs

Solution processes such as spin-coating, inkjet printing, screen printing or spray-printing for OLEDs are still attractive due to their potential advantages for reducing a cost dramatically in the production of large area devices, although vacuum deposition processes are far ahead of solution processes from the commercialization point of view. However, solution processes have an intrinsic disadvantage. The solvent used in the next layer may damage the previous layer, which is the main problem for the solution-processed multilayer structure. One straightforward way to fabricate multilayer structure OLEDs by the solution process is to find the suitable solvents for each layer so that the later solvent will not dissolve the former layer. For that, many researchers have directed their attentions to the cross-linkable [14] or water/alcohol soluble materials [15].

Conjugated polymers have been studied as the solution-processable emitting materials since first PLEDs reported by R. H. Friend's group. Typical polymers used in PLEDs include derivatives of PPV and polyfluorene. While PPV itself is insoluble and difficult to process, a number of PPVs and related poly(naphthalene vinylene)s (PNVs) that are soluble in organic solvents or water have been prepared via ring opening metathesis polymerization. These polymers show different properties depending on the substitution of side chains onto the polymer backbone and the conjugation length; the color of emitting-light, stability and solubility.

Charge injections from electrodes are also important issues on solution-processed OLEDs. For a hole injection, poly(3,4-ethylenedioxythiophene):polystyrene sulfonate (PEDOT:PSS) is widely used in many years. PEDOT:PSS reduces a hole injection barrier between ITO electrode and HTL and is also used for HTL. And it reduces the roughness of ITO electrode. However, PEDOT:PSS has several disadvantages [16]. Recently, soluble metal oxides such as molybdenum oxide (MoO_3) [17], vanadium pentoxide (V_2O_5) [18], tungsten oxide (WO_3) [19] are reported, that are already showed good hole injection abilities in small molecule organic devices based on a vacuum deposition [20,21,22].

For increasing electron injection efficiencies in fabrication of vacuum-deposited OLEDs, a thin layer of lithum fluoride (LiF) is inserted or low work function metal is introduced such as Ba, Ca between ETL and Al [23,24]. These materials are difficult to use in a solution process. For the solution process, zinc oxide (ZnO) is usually used for the electron injection layer (EIL) [25]. But in this case, metal oxides have little high work function for an efficient electron injection because the lowest unoccupied orbital (LUMO) level of light emitting polymers is typically 2–3 eV. So the emitting polymers having high LUMO are used. Recently, it is found that water/alcohol soluble conjugated polymers (WSCPs) with polar pendant groups can improve a charge injection from metallic electrodes into organic active layers resulting in significant enhancement in the device performance [26]. Due to these advantages, more and more efforts have been put in this area and significant progresses have been made in recent years.

One of the precise methods for the deposition of electrodes in the solution process is ink-jet printing. Ink-jet printing is a very attractive technique to deposit materials for electrodes because it can be printed without high-vacuum systems. Many different functional inks have been developed. Recently, inks containing metallic nanoparticles, suitable for ink-jetting, have been received much interest. Several companies now offer inks containing silver nanoparticles. This material is preferred for ink-jet applications because they do not grow insulating oxides when deposited in the presence of oxygen. Although silver nanoparticles inks are currently used in research and in many industrial applications, the growing price of silver may be a problem. For this reason, recently several researches have tried to develop alternative printable inks based on low-cost materials.

1.3 Outline of Thesis

This thesis is composed of five chapters including **Introduction** and **Conclusion**. As an introductory part, **Chapter 1** provides the previous studies of organic light-emitting diodes and solution-processed PLEDs. In **Chapter 2**, preparation methods of ZnO nanoparticles and ink-jet printing systems used in this study are described. Also, the fabrication and characterization methods for the PLEDs are described in detail in this chapter. **Chapter 3** contains the fabrication of the conventional-structured PLEDs with the various solution-processed electron transport layers. PLEDs with n-doped ETL showed good performances with a silver electrode. Two kinds of conjugated polyelectrolyte materials, PEO and PFN-P1, are used for a solution-processed electron transport layer. Among PLEDs using the two materials, the devices with PFN-P1 layer showed compatible performances with n-doped ETL. Finally, we demonstrated all solution-processed PLEDs using the n-doped ETL. In **Chapter 4**, we fabricated solution-processed inverted PLEDs. For that, self-assembled monolayer is used for improving electron injection. In order to increasing more the performance of solution-processed inverted PLEDs, a PFN-P1 layer which is effective in the conventional PLEDs is introduced. For a solution-processable HIL, three materials are introduced in inverted PLEDs; MoO_3 nanoparticles, PEDOT:PSS and sol-gel V_2O_5. Finally, we demonstrated all solution-processed inverted PLEDs using sol-gel V_2O_5 which shows best performances in three materials. And then, some concluding remarks and

suggestion of further study for all solution-processed PLEDs are described in **Chapter 5**.

Chapter 2. Experimental Methods

2.1 Materials

2.1.1 Preparation of ZnO nanoparticles and precursor solution

The ZnO nanoparticles (NPs) were prepared[1] modifying the method reported by C. Pacholski *et al.* [27]. At first, 1.23 g of $Zn(Ac)_2 \cdot 2H_2O$ was dissolved in 55 ml of methanol at room temperature. Then, 25 ml of a methanol solution containing 0.48 g of KOH was added dropwise at 60 ℃ with magnetic stirring. The reaction mixture was kept at 60 ℃ with magnetic stirring for 2 hours under N_2 flow. The product appeared as white precipitate. After collecting by centrifugation, this white precipitate was washed with methanol. Finally, the precipitate could be redispersed in n-butanol. For determining the ZnO concentration, a known amount of the colloidal solution was dried and the residual powder was weighed.

For the ZnO precursor solution, zinc acetate dehydrate ($Zn(CH_3COO)_2$, 99.999%), ethanolamine (EA; $NH_2CH_2CH_2OH$, 99%), chlorobenzene (C_6H_5Cl, anhydrous, 99.8%), methanol (CH_3OH, 99.8%), isopropyl alcohol (C_3H_8O, 99.9%), and acetone ($(CH_3)_2CO$, 99.5%) were purchased from Sigma-Aldrich

[1] The synthesis of ZnO nanoparticles used in this thesis was conducted by Dr. Insun Park, Jaehoon Lim, Prof. Do Yeung Yoon, Prof. Seonghoon Lee and Prof. Kookheon Char in Seoul National University.

Chemical Co., Inc. The ZnO precursor solution was prepared [28] by dissolving zinc acetate dehydrate (0.5487 g, 0.5 molar) in methanol (5 ml) and equal-molar ethanolamine (0.15 ml). The mixed solution was then stirred at 55 ℃ for 1 hour to obtain a transparent mixture, after which it was aged for 48 hours at room temperature.

2.1.2 Preparation of other materials

The materials for vacuum evaporation such as MoO_3, lithium quinolide (Liq), Al and Ag were purchased from CERAC. For n-doped ETL, an electron transport material, tris[3-(3-pyridyl)mesityl]borane (3TPYMB), was purchased from LumTec and a dopant material, KBH_4, was purchased from Sigma-Aldrich. The conjugated polyelectrolyte materials used in this thesis, poly(ethylene oxide) (PEO) and poly[(9,9-bis(3′ -(N,N-dimethyl)-propyl)-2,7-fluorenene)-alt-2,7-(9,9-dioctyfluorene)] (PFN-P1), were purchased from Sigma-Aldrich and 1-material, respectively. The hole injection materials for a solution process, MoO_3 nanoparticles and sol-gel V_2O_5, were purchased from Nanograde GmBH and Alfa Aesar, respectively.

2.2 Ink-jet printing

The ink-jet printing in this thesis was performed by using piezoelectric ink-jet printer UJ200 from Unijet. 30 μm radius nozzle (purchased from Samsung) was used. The Ag precursor ink was purchased from InkTec and Ag nanoparticle ink was purchased from ANP and Sigma-Aldrich. To obtain the well-inkjet-deposited electrodes, many ink-jetting and thermal conditions are optimized including sintering temperature, substrate temperature and voltage waveforms. Substrate temperature was fixed 60 ℃ during jetting. Jetting frequency and nozzle height was 1,000 Hz and 100 μm, respectively. Substrate was annealed at 120 ℃ in N_2 atmosphere or vacuum for 10 min after jetting.

2.3 Device Fabrication and Characterization Methods

2.3.1 Device fabrication

All devices used in this thesis have slightly different structures in each chapter to obtain optimized performances. Specified device structures, process or chemical materials are described in each chapter. Typical device fabrication methods are as follows: The ITO patterned glass substrates were cleaned in ultrasonic bath (Branson 5510) with acetone, isopropyl alcohol (IPA) and deionized (DI) water. The cleaned substrates were dried in ambient oven at 120 ℃ for more than 2 hours. For the standard structure, the ITO patterned glass substrates were treated with ultraviolet-ozone cleaner (UVO-42) to remove the surface hydrocarbon contamination and increase the work function of ITO when we employed PEDOT:PSS (CLEVIOS™ P VP AI 4083, H. C. Starck) as a hole injecting layer (HIL). PEDOT:PSS film is deposited by spin-coating at a speed of 4,000 rpm for 30 sec in Ar atmosphere and then dried in same atmosphere on hotplate at 145 ℃ for 10 min. For the inverted structure, the ITO patterned glass substrates were not UV-ozone treated and on top of that, a ZnO layer was deposited by spin-coating at a speed of 2,000 rpm for 60 sec, followed by drying in N_2 oven at a temperature of 90 ℃ for 30 min.

Light-emitting polymers are deposited by spin-coating. We used toluene and chlorobenzene for solvents diluting those polymers. Detailed reasons for

using two solvents are described in later. The red and green polymers, SPR-001 and SPG-01T, are spin-coated at a speed of 2,000 rpm for 60 sec. The yellow polymer, PDY-132, is spin-coated at a speed of 2,500 rpm for 60 sec. The blue polymer, SPB-02T, is spin-coated at a speed of 3,000 rpm for 60 sec. All coated films are dried on hotplate at 120 ℃ for 30 min in Ar atmosphere.

The vacuum deposition of thin films was performed by thermal evaporation under a base pressure of 0.05–0.08 Å/s for Liq (electron injecting material), 0.2–0.5 Å/s for MoO_3 (hole injecting material) and 3–6 Å/s for Al and Ag (metal cathode), respectively. The evaporation speed was monitored with a quartz-oscillator thickness monitor. The emitting area is 1.4 × 1.4 mm^2 which is defined by the crossing overlap of anode and cathode.

2.3.2 Current-voltage-luminance measurement

Fabricated device was mounted onto the cryostat for the current-voltage-luminance (I-V-L) measurement. The devices were measured at room temperature. The current-voltage (I-V) characteristics were measured with a Keithley 236 source measurement unit, while the electroluminescence was measured with a calibrated Si photodiode (Hamamatsu, S5227-1010BQ) with a size of 10 mm × 10 mm placed at an angle normal to the device surface, assuming that the device was a Lambertian source. To detect a turn-on voltage of light-emitting diodes, we use an ARC PD438 photomultiplier tube (PMT) with the Keithley 236 source measurement unit. The EL spectra and the Commission Internationale de L'Eclairage (CIE) color coordinates were

measured with a Konica-Minolta CS-1000A spectroradiometer. The luminance and efficiency were calculated from the photocurrent signal of photodiode with a Keithley 2000 multimeter, and corrected precisely with the luminance from CS-1000A. The schematic diagrams of I-V-L and EL spectra measurement are shown in Figure 2.1.

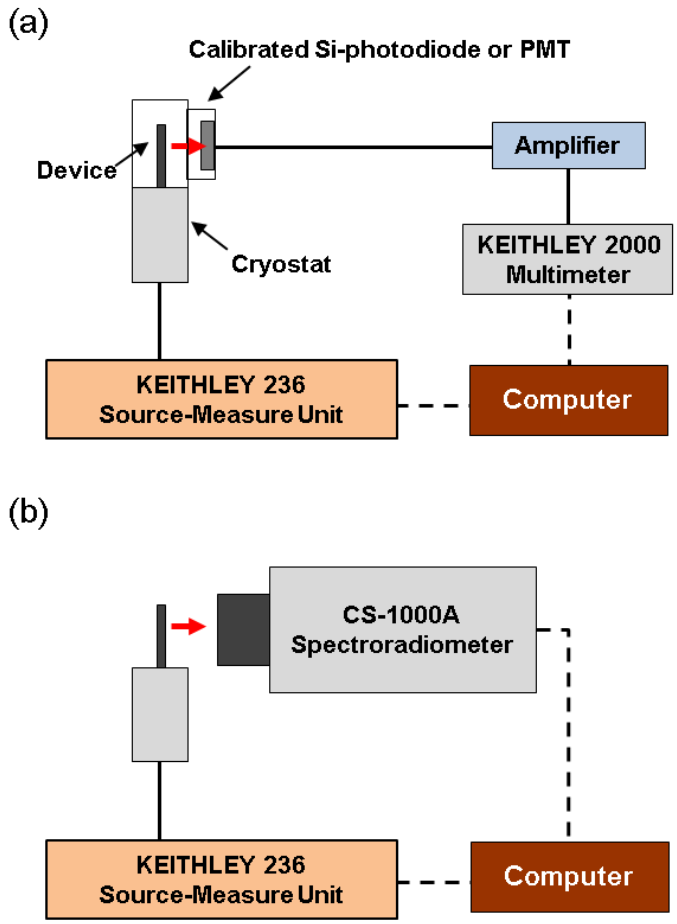

Figure 2.1 The schematic diagrams for the measurement of (a) I-V-L characteristics and (b) EL spectra.

The chromatic characteristics were calculated from EL spectra measured by the CS-1000A spectrometer using the CIE 1931 color expression system. The tristimulus values *XYZ* can be calculated by following equations,

$$X = K_m \int_0^\infty \bar{x}(\lambda) P(\lambda) d\lambda \quad (2.1)$$

$$Y = K_m \int_0^\infty \bar{y}(\lambda) P(\lambda) d\lambda \quad (2.2)$$

$$Z = K_m \int_0^\infty \bar{z}(\lambda) P(\lambda) d\lambda \quad (2.3)$$

where, $P(\lambda)$ is a given spectral power distribution of emissive source, $\bar{x}$, $\bar{y}$ and $\bar{z}$ are the CIE standard color matching functions (see Figure 2.2) and K_m is the weighing constant (683 lm W^{-1}). From the tristimulus values, the CIE color coordinates calculated by following equations,

$$x = \frac{X}{X+Y+Z} \quad (2.4)$$

$$y = \frac{Y}{X+Y+Z} \quad (2.5)$$

$$z = \frac{Z}{X+Y+Z} \quad (2.6)$$

Any color can be plotted on the CIE chromaticity diagram.

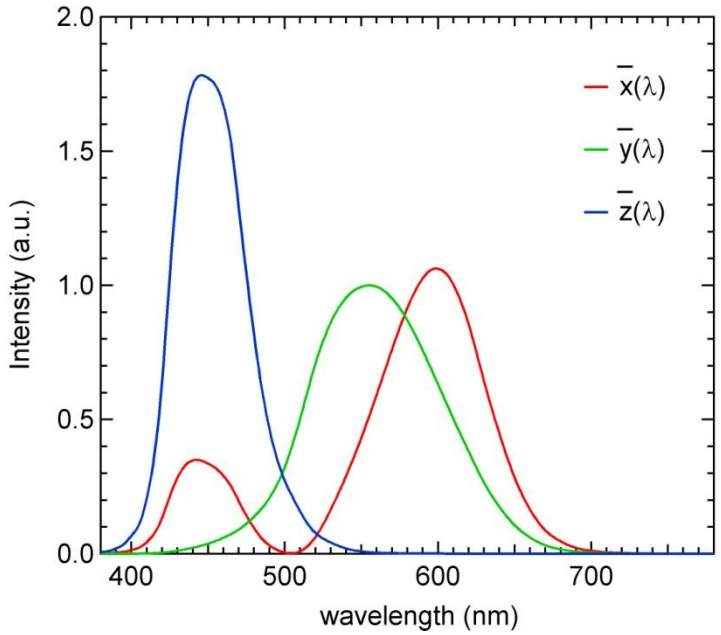

Figure 2.2 The CIE standard observer color matching functions.

2.3.3 Emission efficiency calculation

To evaluate the emission properties of light-emitting diodes, the commonly employed efficiencies are the EQE, the luminous efficiency (LE) and the power efficiency (PE).

The external quantum efficiency can be defined by the following equation.

$$\mathrm{EQE} = \frac{number\ of\ emitted\ photons}{number\ of\ injected\ electrons}(\%)$$

Typically, OLEDs emit light into the half plane due to the metal contact. Without any modification for increasing out-coupling efficiency, over 80% of

the emission can be lost to internal absorption and wave-guiding in a simple planar light-emitting device.

Since human eye has different spectral sensitivity in visible area, the response of the eye is standardized by the CIE in 1924 (see $\bar{y}$ in Figure 2.2). The luminous efficiency weighs all emitted photons according to the photopic response of human eye. The difference is that EQE weighs all emitted photons equally. LE can be expressed by the following equation.

$$\mathrm{LE} = \frac{luminance}{current\ density}(cd/A)$$

The luminance value (cd/m^2) can be easily measured by the commercial luminance meter (CS-1000A in this thesis).

The power efficiency is the ratio of the lumen output to the input electrical power as follows,

$$\mathrm{PE} = \frac{luminous\ flux}{electrical\ power}(lm/W)$$

The EQEs can be useful to understand the fundamental physics for light emission mechanism, while the PEs can be useful to interpret the power dissipated in a light-emitting device when used in a display application.

2.3.4 Other Characterization Methods

UV-Vis. Spectroscopy: The transmission and absorption spectra were measured with DU-70 UV/Vis Scanning Spectrophotometer (Beckman Coulter, Inc.) or Agilent 8454 UV-Vis. diode array spectrometer. For the film measurement, materials were spin-coated on quartz substrate.

Energy Level Measurement: The highest-occupied-molecular-orbital (HOMO) energy levels of organic materials were measured by Model AC-2 Photoelectron Spectrometer (RKI Instruments) in ambient atmosphere at room temperature. The materials were deposited on the ITO coated glass substrate.

Ultraviolet Photoelectron Spectroscopy (UPS): The energy levels of ZnO NPs were measure by AXIS-NOVA (Kratos. Inc) UPS at 3.5×10^{-9} Torr. The metal oxides are deposited on the ITO coated glass substrate using spin-coating.

Thickness of Film Measurement: Ellipsometers (L2W15S830 with 632.8-nm He-Ne laser light, Gaertner Scientific Corp. and M2000D, Woollam) and an AFM (XE-100, Park Systems) were used for measuring the thicknesses of films.

Chapter 3. Solution-processed Polymer Light-Emitting Diodes with a Conventional Device Structure

3.1 Characteristics of red, yellow, green and blue PLEDs

3.1.1 Light-emitting polymers

For the fabrication of solution-processed PLEDs, light-emitting polymers were purchased from Merk. The polymers are SPR-001 for red, PDY-132 for yellow, SPG-01T for green and SPB-02T for blue. Absorption spectra and photoluminescent (PL) spectra are shown in Figure 3.1. The red light-emitting polymer (SPR-001) is a spiro-copolymer with peak absorption at 340 nm, shoulder absorption at 455 nm and peak PL intensity at 635 nm. The yellow light-emitting polymer (PDY-132) is a PPV copolymer with peak absorption at 450 nm and peak PL intensity at 545 nm. The green light-emitting polymer (SPG-01T) is a spiro-copolymer with peak absorption at 395 nm, shoulder absorption at 340 nm, and peak PL intensity at 510 nm. The blue light-emitting polymer (SPB-02T) is a spiro-bifluorene based copolymer with peak 390 nm, shoulder absorption at 340 nm, and peak PL intensity at 480 nm. For measuring absorption spectra and PL, polymers dissolved in toluene are spin-coated onto quartz substrate. The thicknesses of all films are about 80 nm. The

HOMO energy levels and the LUMO energy levels are summarized in Figure 3.2.

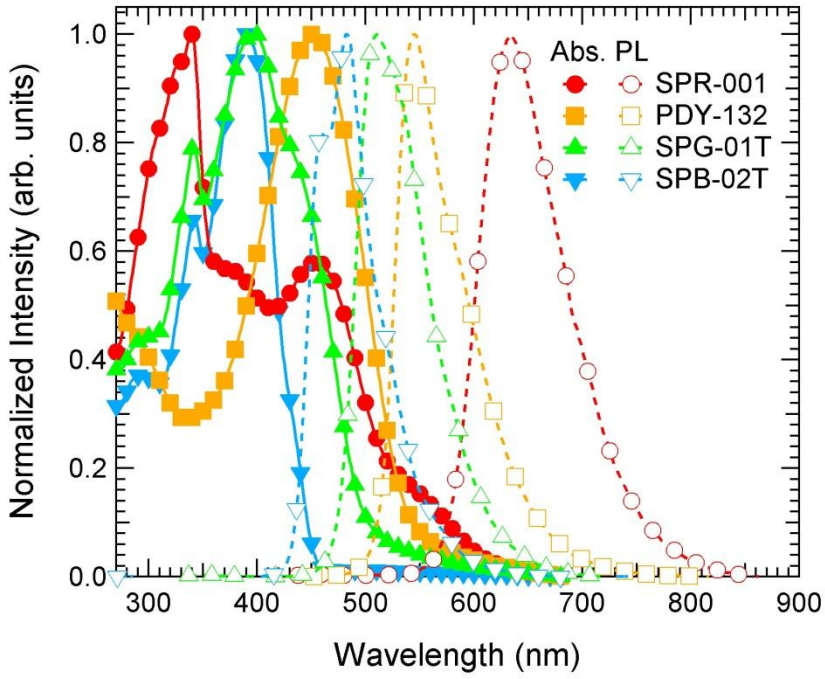

Figure 3.1 The Normalized absorption spectra and PL intensity of light-emitting polymers.

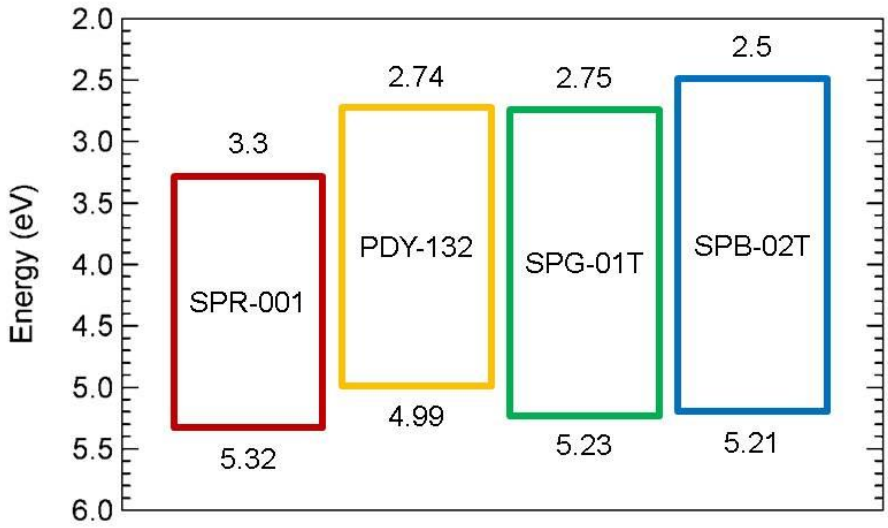

Figure 3.2 The schematic energy level diagrams of light-emitting polymers.

3.1.2 Device characteristics of PLEDs

The basic structure of PLEDs we used is as follows: ITO anode/PEDOT:PSS (40 nm) (HIL)/light-emitting polymers (80 nm) (the light-emitting layer, EML)/Liq (3 nm) (EIL)/Al (100 nm) cathode. For spin-coating polymers, we dissolved all polymers in toluene.

Figure 3.3 shows the current density-voltage (J-V) and luminance-voltage (L-V) characteristics of the devices with various light-emitting polymers. In Figure 3.3(b), we obtained that the turn-on voltage (V_T) of 1.8, 3.2, 3.2 and 3.6 V for red, yellow, green and blue PLEDs, respectively. (We define the turn-on voltage as the voltage at 1 cd/m^2.) The maximum luminances of the red, yellow, green and blue PLEDs are 7,000, 37,000, 4,200 and 3,700 cd/m^2, respectively. The difference of V_T is from the electron

injection barriers between polymers and Liq layer. The Liq layer used as EIL has an electron affinity of 2.8 eV [29]. As shown in Figure 3.2, the LUMO energy levels of red, yellow, green and blue polymers are 3.3, 2.74, 2.75 and 2.5 eV, respectively; having electron injection barriers of -0.6, -0.04, -0.05 and 0.2eV, respectively. So red OLED has the lowest V_T, yellow and green OLEDs have a similar V_T and blue OLED has the highest V_T.

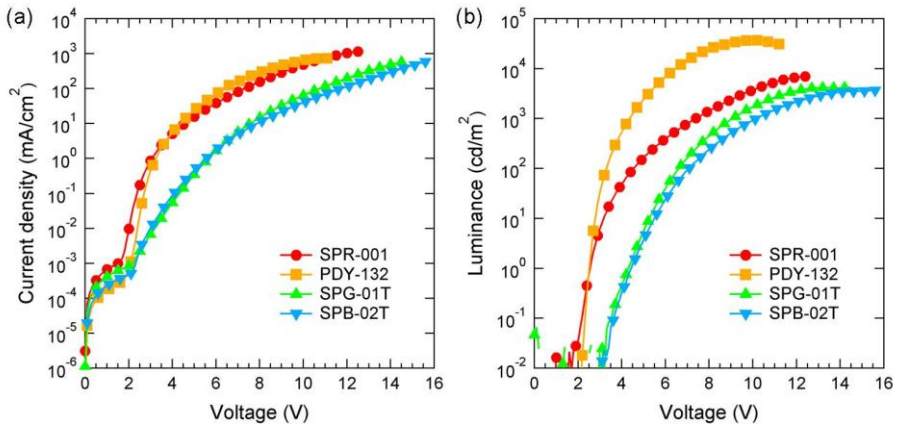

Figure 3.3 (a) J-V and (b) L-V characteristics of the devices with various light-emitting polymers.

EQE-J and LE-J characteristics with various light-emitting polymers are shown in Figure 3.4. The maximum EQE of the red, yellow, green and blue PLEDs are 1.56, 3.24, 0.95 and 1.46%, respectively. And the maximum LE of the red, yellow, green and blue PLEDs are 1.05, 10.14, 3.02 and 2.36 cd/A, respectively. As shown in Figure 3.5, the normalized EL spectra of red, yellow, green and blue PLEDs have the peak EL intensity at 643, 550, 506 and 484 nm, respectively.

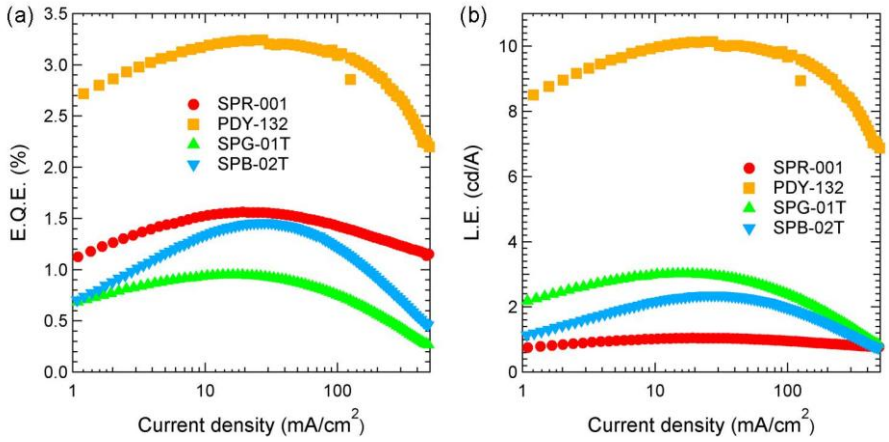

Figure 3.4 (a) EQE-J characteristics and (b) LE-J characteristics with various light-emitting polymers.

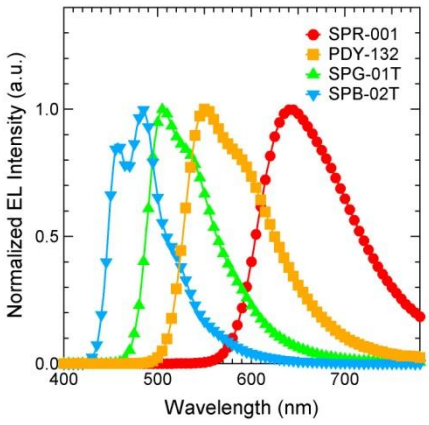

Figure 3.5 The normalized EL spectra at the same current density (J = 51 mA/cm^2) of the devices with various light-emitting polymers.

3.2 PLEDs with a Solution-processed N-type Doped Electron Transport Layer

As mentioned in chapter 1.2, charge injections from electrodes are important issues on PLEDs. If n-type doped ETL is used, the reactions between n-dopant and ETL change an electron transfer characteristics and an electron concentration in n-doped ETL [30]. It results in energy band level changes and vacuum level shifts. So an electron injection is less affected by work function of adjacent electrodes by introducing n-doped ETL. The most widely used n-type dopant for the ETL are alkaline metals, such as cesium and lithium [31,32]. As these alkaline metals are highly reactive, it is difficult handling them and it cannot be applied to a solution process. So some alkaline metal carbonates used as the dopant for n-doped ETL. For that, cesium carbonate (Cs_2CO_3) is generally used. This material can be applied to a thermal evaporation [33] and also a solution process [34]. For the rest, some materials are used for n-dopant, such as cesium azide (CsN_3) [35] and lithium nitride (Li_3N) [36]. There are few n-type doping materials in comparison to p-type doping materials. Moreover, a few n-type dopant materials are used for a solution process.

In this part, we report a method of n-type doping by using KBH_4 for high efficiency PLEDs with solution processes. KBH_4 is reported as an electron injection material [37] and n-dopant [38] by vacuum evaporation. But it is not used n-dopant for solution processes yet. We have been used KBH_4 for n-

dopant by solution process and it works efficiently; the performances of devices are improved. The devices using the KBH_4 doped 3TPYMB layer showed lower turn-on and driving voltages, higher luminance and efficiency compared to the device with non-doped 3TPYMB layer and without any layers.

3.2.1 Device characteristics depending on KBH_4 doping ratio in ETL

The PLEDs had a configuration of ITO/PEDOT:PSS (30 nm)/PDY-132 (80 nm)/3TPYMB:KBH_4 (x%, 30 nm)/Liq (3 nm)/Al (100 nm). PEDOT:PSS and PDY-132 which dissolved in toluene with 5 mg/ml are spin-coated onto ITO patterned glass substrate in sequence as mentioned before. 3TPYMB:KBH_4 layers dissolved in methanol at 0.6 wt% were spin-coated onto the emissive layer in various doping ratios of 10–40%, and then dried on the hot plate in Ar atmosphere at 60 ℃ for 30 min. For the electrodes, Liq and Al were thermally evaporated.

Figure 3.6 shows J-V and L-V characteristics of the devices with a various KBH_4 doping ratio in 3TPYMB. Compared to the device without 3TPYMB layer, the device with 3TPYMB layer shows better performance; lower turn-on voltage, higher efficiency. Hole-electron recombination in device without ETL typically occurs near the electrode. Excitons formed near an electrode have a strong probability of decaying via a nonradiative path due to their dipole interaction with the metallic electrode. These nonradiative

recombination further decrease EQE of the device. However, Due to inserting this 3TPYMB layer, electrons inject efficiently to EML and hole-electron recombination zone is move away from the cathode electrode. It enhances the probability of radiative exciton recombination. The current density and luminance of the device more increase by KBH_4 doping in 3TPYMB up to 30% and then somewhat decrease.

As shown in Figure 3.7, EQE and LE of the devices also increase. For the device with 30% of KBH_4 doping ratio, the driving voltage for 1000 cd/m^2 is 2.9 V, the maximum luminance is 102,600 cd/m^2 at 11.4 V, the maximum EQE is 5.21 % at 2.4 V and the maximum LE is 14.92 cd/A at 2.4 V. It means that the device with 30% of KBH_4 have 33% lower driving voltage, 3.7 times higher maximum luminance, 13% higher maximum EQE and 10% higher maximum LE than the device with non-doped 3TPYMB. We summarize the performance of OLEDs with different KBH_4 doping concentrations in Table 3.1. These results indicate that the injection and transport of electrons become better as increasing the doping ratio of KBH_4 in 3TPYMB and electron-hole balance becomes to be improved.

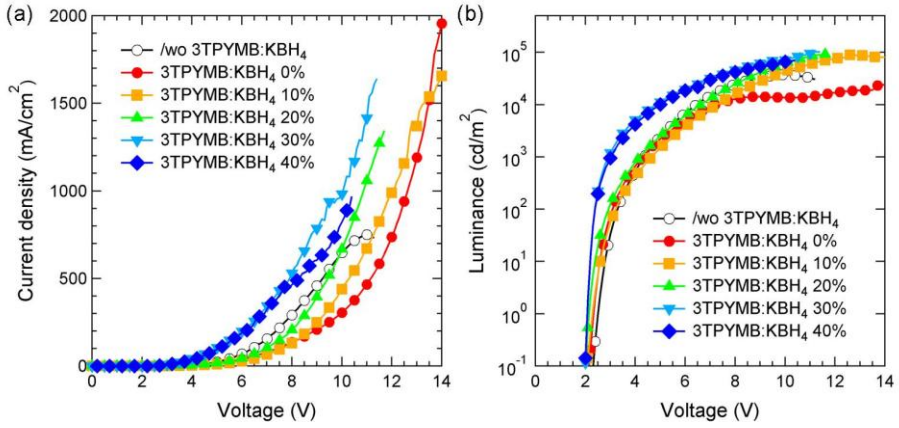

Figure 3.6 (a) J-V and (b) L-V characteristics of the devices without n-doped ETL and with ETLs having different KBH_4 doping ratio in 3TPYMB.

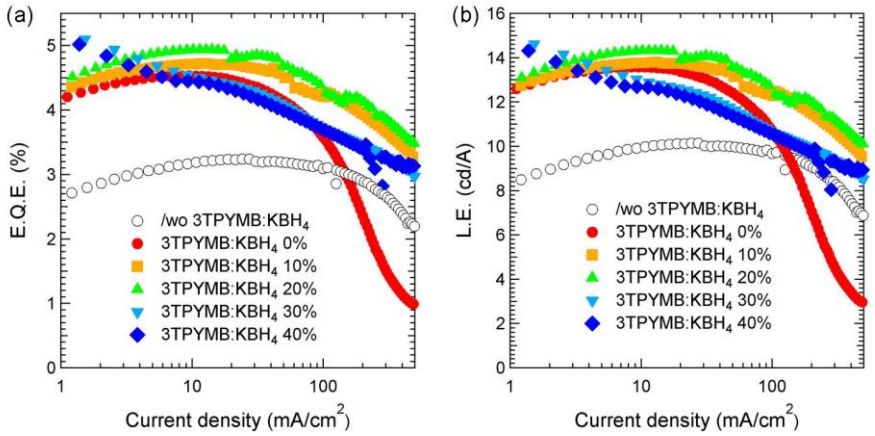

Figure 3.7 (a) EQE-J and (b) LE-J characteristics of the devices without n-doped ETL and with ETLs having different KBH_4 doping ratio in 3TPYMB.

Figure 3.8 shows the EL spectra, normalized at the main emission peak (~553 nm), for the devices with different KBH_4 doping ratio at a current density of 51 mA/cm^2. The emission peak at ~590 nm is rising with increasing the KBH_4 doping ratio. This can be also attributed to the shift of the electron-hole recombination zone; it induces the change of electroluminescent characteristics.

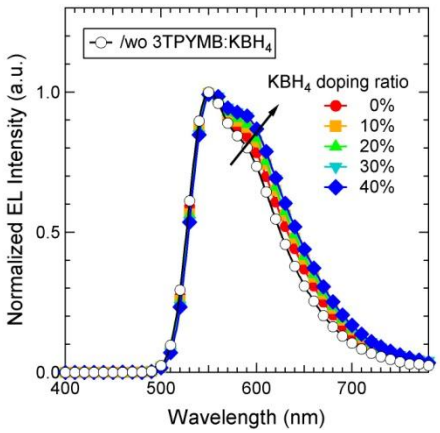

Figure 3.8 The normalized EL spectra at the same current density (J = 51 mA/cm^2) of the devices without n-doped ETL and with ETLs having different KBH_4 doping ratio in 3TPYMB.

Table 3.1 Performance of OLEDs with different KBH_4 doping concentrations.

Electron tansport layer	Driving voltage[a] (V)	Maximum Luminance (cd/m^2)	Maximum EQE (%)	Maximum LE (cd/A)
Non	4.4	37,000	3.24	10.14
3TPYMB:KBH_4 0%	4.3	27,500	4.53	13.58
3TPYMB:KBH_4 10%	4.6	90,500	4.72	13.80
3TPYMB:KBH_4 20%	4.2	91,400	4.94	14.33
3TPYMB:KBH_4 30%	2.9	102,600	5.21	14.92
3TPYMB:KBH_4 40%	3.0	71,100	5.22	14.89

[a]At luminance of 1000 cd/m^2.

3.2.2 UPS measurement of KBH_4 doped 3TPYMB layer

We measured the UPS spectra of the non-doped 3TPYMB and 30% KBH_4 doped 3TPYMB films to understand the role of KBH_4 in improving the electron injection and transport properties as shown in Figure 3.9. The HOMO level of pristine 3TPYMB film is located about 2.7 eV below the Fermi level (i.e., 6.8 eV), which corresponds to the reported value [39]. The LUMO level calculated from the bandgap is 3.2 eV, about 0.9 eV apart from the Fermi level. On the other hand, the HOMO level of KBH_4 doped 3TPYMB film locates at

7.1 eV from the vacuum level. From the optical band gap, the Fermi level is only 0.1 eV below from the LUMO level, showing that KBH_4 acts as the n-dopant in 3TPYMB. In addition, the cutoff edge of 3TPYMB shifted to the higher binding energy by 0.5 eV after doping KBH_4 as can be seen in Figure 3.10. It means that the vacuum level was shifted by the dipole moment, and thus, electron injection can be enhanced at the interface.

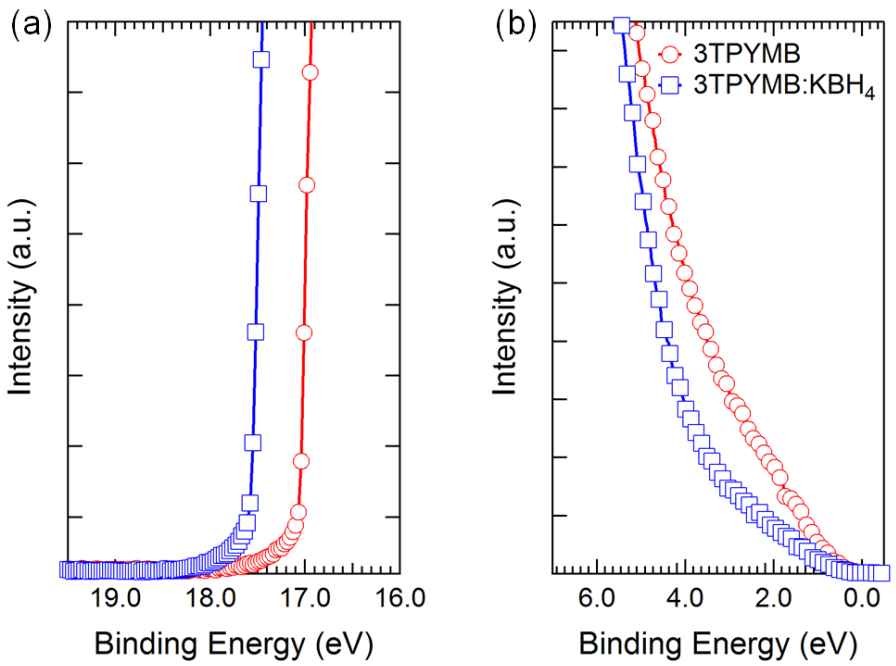

Figure 3.9 UPS spectra of 3TPYMB and 3TPYMB:KBH_4 near (a) the secondary electron cutoff region and (b) the valence band regions.

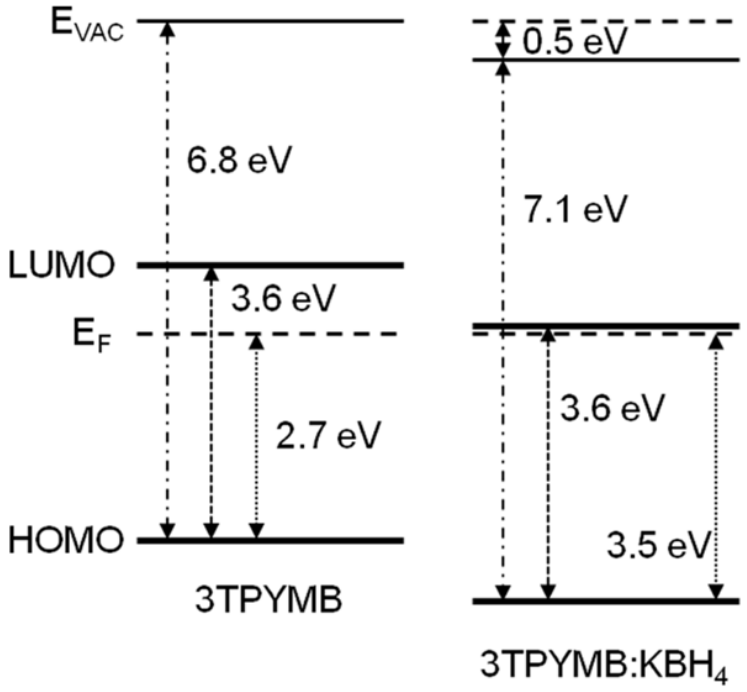

Figure 3.10 Schematic energy level diagrams of pristine 3TPYMB and 3TPYMB:KBH_4 films.

3.2.3 Device characteristics of red, green and blue PLEDs with a KBH_4 doped 3TPYMB layer

To investigate the effect of the n-type doped ETL in the PLEDs, red, green and blue devices were fabricated with following structures:

R1: ITO/PEDOT:PSS (30 nm)/SPR-001 (80 nm)/Liq (3 nm)/Al (100 nm)

R2: ITO/PEDOT:PSS (30 nm)/SPR-001 (80 nm)/3TPYMB:KBH_4 (30%, 30 nm)/Liq (3 nm)/Al (100 nm)

G1: ITO/PEDOT:PSS (30 nm)/SPG-01T (80 nm)/Liq (3 nm)/Al (100 nm)

G2: ITO/PEDOT:PSS (30 nm)/SPG-01T (80 nm)/3TPYMB:KBH_4 (30%, 30 nm)/Liq (3 nm)/Al (100 nm)

B1: ITO/PEDOT:PSS (30 nm)/SPB-02T (80 nm)/Liq (3 nm)/Al (100 nm)

B2: ITO/PEDOT:PSS (30 nm)/SPB-02T (80 nm)/3TPYMB:KBH_4 (30%, 30 nm)/Liq (3 nm)/Al (100 nm)

Figure 3.11 and Figure 3.12 shows the device performances of the red, green and blue PLEDs with KBH_4 doped 3TPYMB layer. In general, the devices with n-doped ETL show better performance; lower turn-on voltage, lower operating voltage, higher maximum luminance and higher efficiencies. In case of red PLED, the operating voltage is increasing with n-doped ETL. Before inserting that layer, electron inject well from cathode electrode to SPR-001 layer. There is no electron injection barrier between EML and cathode. However, the total thickness of the device is increased by inserting this KBH_4 doped 3TPYMB layer. So turn-on voltage and operating voltage is increased.

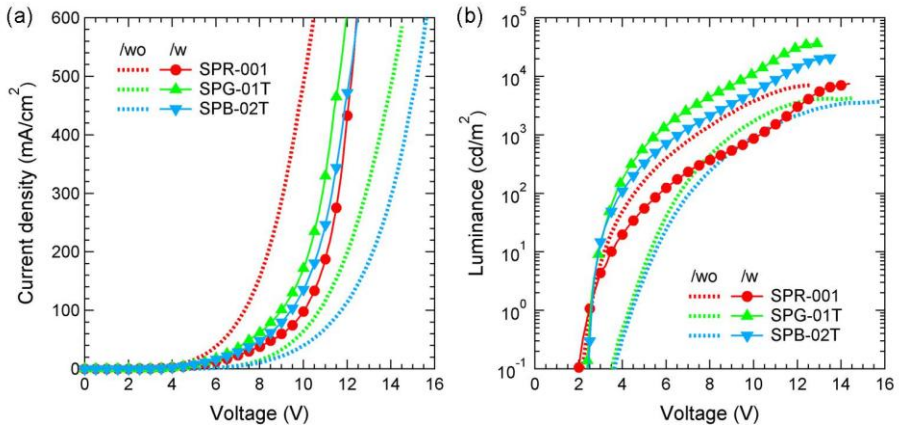

Figure 3.11 (a) J-V and (b) L-V characteristics of the red, green and blue PLEDs without or with KBH_4 doped 3TPYMB layer.

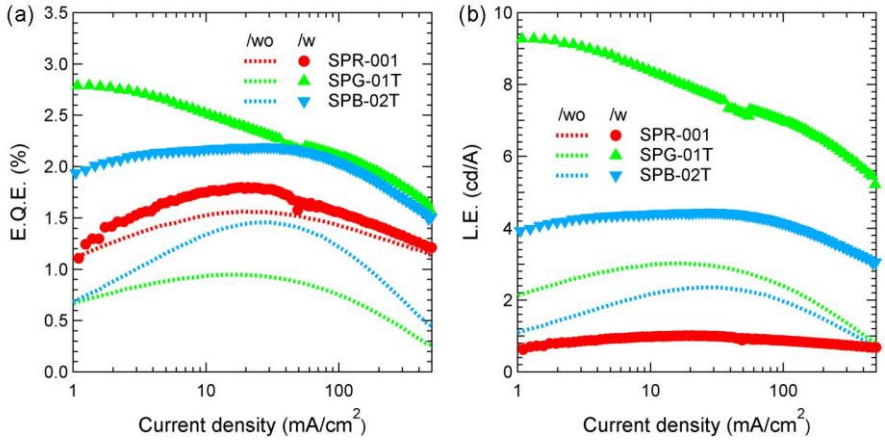

Figure 3.12 (a) EQE-J and (b) LE-J characteristics of the red, green and blue PLEDs without or with KBH_4 doped 3TPYMB layer.

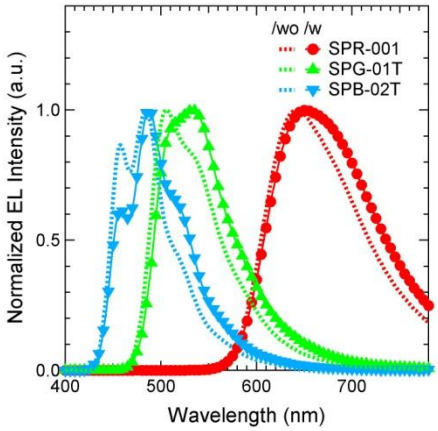

Figure 3.13 The normalized EL spectra at the same current density (J = 51 mA/cm^2) of the red, green and blue PLEDs without or with KBH_4 doped 3TPYMB layer.

As shown in Figure 3.12, the maximum EQEs are 1.80, 2.79 and 2.19% in red, green and blue PLEDs with KBH_4 doped 3TPYMB layer, respectively. And the maximum LEs are 1.05, 9.28 and 4.45 cd/A in red, green and blue PLEDs with KBH_4 doped 3TPYMB layer, respectively. These values are higher than the maximum EQE and LE of red, green and blue OLEDs without n-doped ETL. (red: 1.56%, 1.01 cd/A, green: 0.95%, 3.02 cd/A and blue: 1.46%, 2.36 cd/A) These better performances were attributed to more efficient electron injection due to introducing the KBH_4 doped 3TPYMB layer.

Figure 3.13 shows the changing of EL spectra by introducing n-doped ETL. Efficient electron injection cause shifting of the recombination zone; the peak emission wavelength is red-shifted. We summarize the performance of red, green and blue PLEDs with KBH_4 doping in Table 3.2.

Table 3.2 The device performances of red, green and blue PLEDs without or with KBH_4 doped 3TPYMB layer.

	Red OLED		Green OLED		Blue OLED	
	/wo	/w	/w	/w	/wo	/w
Max. Luminance (cd/m^2)	7,000	7,500	4,200	36,000	3,700	20,700
Max. EQE (%)	1.56	1.80	0.95	2.79	1.46	2.19
Max. LE (cd/A)	1.01	1.05	3.02	9.28	2.36	4.45
EL λ_{max} (nm)	643	651	506	532	484	487

3.2.4 Device characteristics of red, yellow, green and blue PLEDs with a KBH_4 doped 3TPYMB layer and Ag cathode

As mentioned before, it is difficult to deposit Liq and Al layers by solution process. And ink-jet printing of Ag is usually used for deposition of solution-processed cathode electrode. To investigate the possibility of all solution-

processed PLEDs with n-type doped ETL, red, yellow, green and blue devices were fabricated with following structures:

R3: ITO/PEDOT:PSS (30 nm)/SPR-001 (80 nm)/Ag (100 nm)

R4: ITO/PEDOT:PSS (30 nm)/SPR-001 (80 nm)/3TPYMB:KBH_4 (30%, 30 nm)/Ag (100 nm)

Y3: ITO/PEDOT:PSS (30 nm)/SPR-001 (80 nm)/Ag (100 nm)

Y4: ITO/PEDOT:PSS (30 nm)/SPR-001 (80 nm)/3TPYMB:KBH_4 (30%, 30 nm)/Ag (100 nm)

G3: ITO/PEDOT:PSS (30 nm)/SPG-01T (80 nm)/Ag (100 nm)

G4: ITO/PEDOT:PSS (30 nm)/SPG-01T (80 nm)/3TPYMB:KBH_4 (30%, 30 nm)/Ag (100 nm)

B3: ITO/PEDOT:PSS (30 nm)/SPB-02T (80 nm)/Ag (100 nm)

B4: ITO/PEDOT:PSS (30 nm)/SPB-02T (80 nm)/3TPYMB:KBH_4 (30%, 30 nm)/Ag (100 nm)

Silver has a high work function about 4.9 eV; electron is difficult to inject from this silver cathode to EML directly. Electron injection barrier is so high about 1.6, 2.16, 2.15 and 2.4 eV, when using red, yellow, green and blue polymer, respectively. So the device performances of PLEDs without any layers between EML and cathode are poor. As shown in Figure 3.15(a), the maximum EQEs of PLEDs using Ag cathode without any layers between EML and cathode are 0.10, 0.08, 0.23 and 0.27% in red, yellow, green and

blue OLEDs. Those values are much low than the EQEs of devices using Liq/ Al bilayer. (red: 1.56%, yellow: 3.24%, green: 0.95% and blue: 1.46%)

Though PLEDs using Ag cathode have a very high electron injection barrier and poor device performances, device performances are dramatically increased by introducing KBH_4 doped 3TPYMB layer between EML and Ag cathode. The electron injection barrier between KBH_4 doped 3TPYMB layer and Ag cathode still high, so the operating voltage of the devices are increased as shown in Figure 3.14(a). However the exciton formation is increased due to increased electron charge by introducing n-doped ETL. So the luminance and efficiencies are successfully increased in PLEDs with the KBH_4 doped 3TPYMB layer as shown in Figure 3.14(b) and Figure 3.15. The detailed performances of red, yellow, green and blue devices with n-doped ETL are summarized in Table 3.3. And Figure 3.16 shows red-shift of EL spectra by introducing KBH_4 doped 3TPYMB layer between EML and Ag cathode.

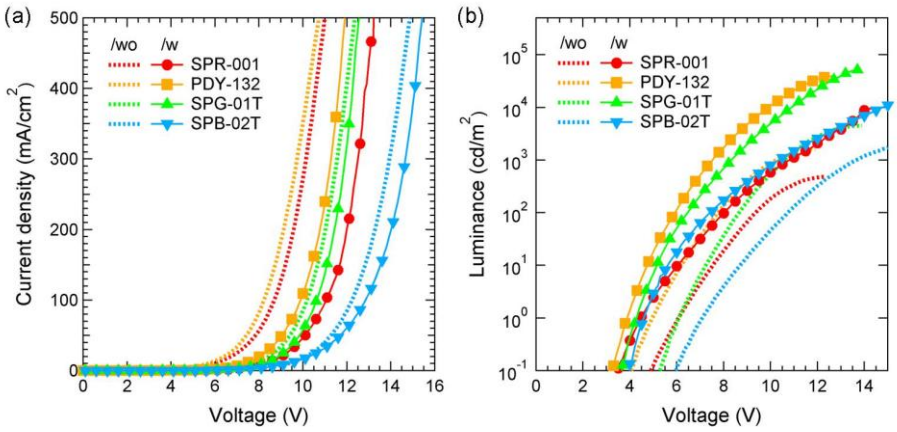

Figure 3.14 (a) J-V and (b) L-V characteristics of the red, yellow, green and blue PLEDs using Ag cathode without or with KBH_4 doped 3TPYMB layer.

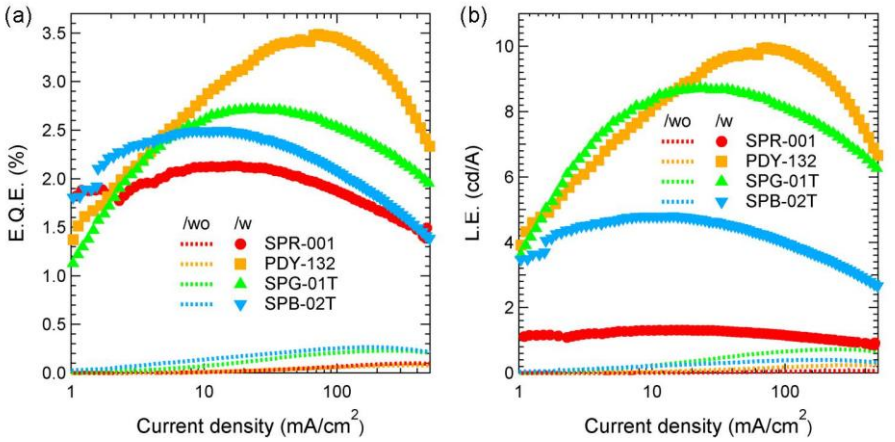

Figure 3.15 (a) EQE-J and (b) LE-J characteristics of the red, yellow, green and blue PLEDs using Ag cathode without or with KBH_4 doped 3TPYMB layer.

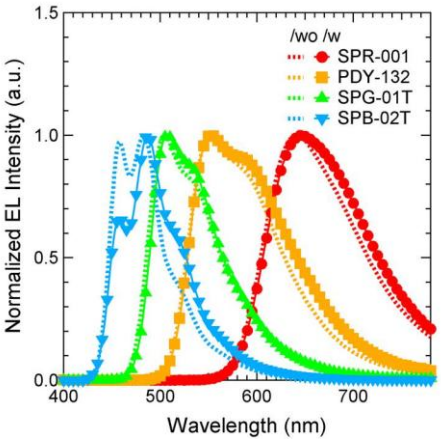

Figure 3.16 The normalized EL spectra at the same current density (J = 51 mA/cm^2) of the red, yellow, green and blue PLEDs using Ag cathode without or with KBH_4 doped 3TPYMB layer.

Table 3.3 The device performances of red, yellow, green and blue PLEDs using Ag cathode with KBH_4 doped 3TPYMB layer.

	Red	Yellow	Green	Blue
Max. Luminance (cd/m^2)	9,600	39,600	51,700	17,800
Max. EQE (%)	2.13	3.49	2.72	2.50
Max. LE (cd/A)	1.31	9.95	8.72	4.80
EL λ_{max} (nm)	646	553	507	487

Device performances are improved in terms of lower driving voltage, higher luminance, and higher efficiency in PLEDs adopting 3TPYMB:KBH_4 layer, irrespective of the cathode electrodes. It can be seen in Figure 3.17. These results indicate that the injection and transport of electrons become better by introducing KBH_4 doped 3TPYMB layer and electron-hole balance becomes to be improved.

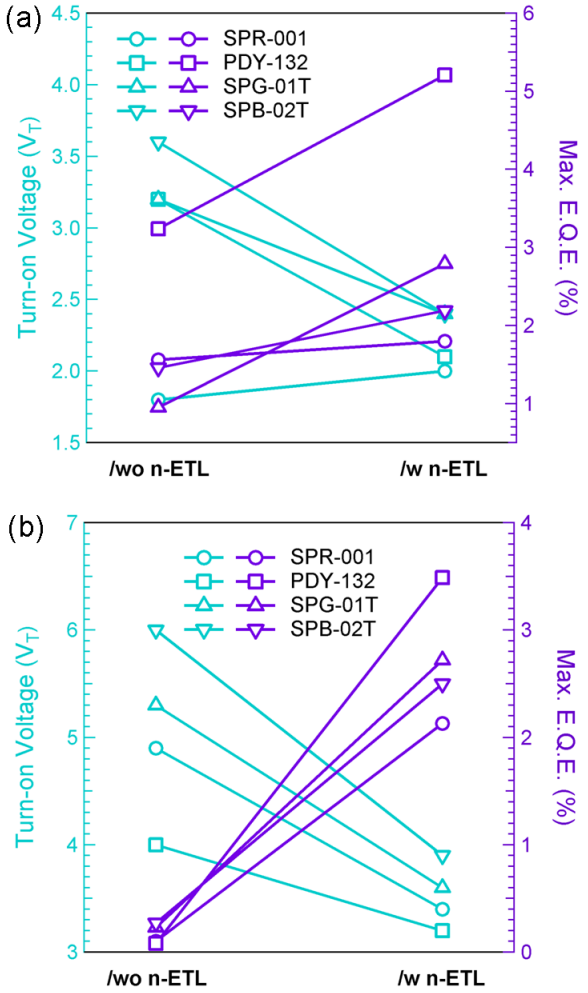

Figure 3.17 Turn-on voltage and maximum EQE of the red, yellow, green and blue PLEDs adopting 3TPYMB:KBH_4 layer with (a) Liq/Al cathode and (b) Ag cathode.

3.3 PLEDs with a Solution-processed Conjugated Polyelectrolyte

Recently, it found that WSCPs can improve charge injection from metallic electrodes into organic active layers resulting in enhancement in the device performance as mentioned before. So we fabricated PLEDs with two conjugated polyelectrolyte materials, PEO and PFN-P1, for improving electron injection efficiency.

3.3.1 Device characteristics depending on PEO thicknesses

The PLEDs consist of an ITO anode, a 30 nm PEDOT:PSS, a 80 nm PDY-132 polymer layer, a PEO layer and a Liq (3 nm)/Al (100 nm). For investigating on device performance depending on thickness of PEO, PEO is dissolved in acetonitrile at various concentrations of 0.1–2 mg/ml and it is spin-coated onto the emissive layer. Then the PEO layer is dried on the hot plate in Ar atmosphere at 80 ℃ for 30 min.

Figure 3.18 shows J-V and L-V characteristics of the devices with a various concentrations of PEO. Compared to the device without PEO layer, the device with PEO layers in 0.1, 0.3, 0.5 mg/ml shows lower operating voltages. Conjugated polyelectrolyte is known as lowering charge injection barriers by the formation of an interfacial dipole [40]. By introducing PEO layer up to 0.5 mg/ml, the operating voltages are decreased. But increasing

more the concentration of PEO makes too thick films; the operating voltages are increased.

As shown in Figure 3.19, EQE and LE of the devices increase in the PEO concentration of 0.5 mg/ml. That is the optimum concentration of PEO. For the device with 0.5 mg/ml of PEO concentration, the driving voltage for 1000 cd/m^2 is 3.7 V, the maximum luminance is 20,200 cd/m^2 at 7.5 V, the maximum EQE is 4.48% and the maximum LE is 14.00 cd/A. These results indicate that the PEO layer lowering an electron injection barrier and transport of electrons become well; electron-hole balance becomes to be improved. As shown in Figure 3.20, the EL spectra normalized at the main emission peak (550 nm) have no difference with different PEO concentrations at a current density of 51 mA/cm^2.

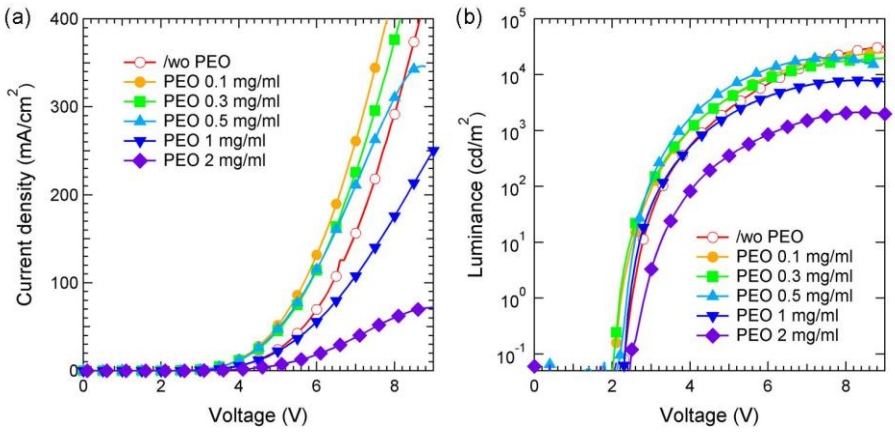

Figure 3.18 (a) J-V and (b) L-V characteristics of the devices with a various concentrations of PEO.

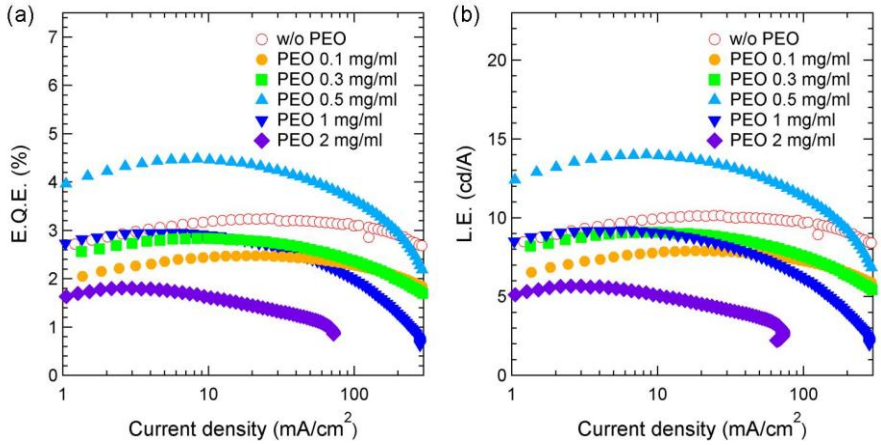

Figure 3.19 (a) EQE-J and (b) LE-J characteristics for the devices with different PEO concentrations.

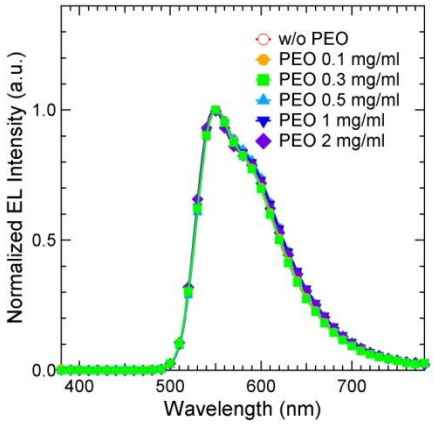

Figure 3.20 The normalized EL spectra at the main emission peak (550 nm) for the devices with different PEO concentrations at a same current density of 51 mA/cm^2.

3.3.2 Device characteristics of PLEDs with PEO and Ag cathode

Similar to KBH_4 doped 3TPYMB layers, PEO layer is introduced in red, yellow, green and blue devices with Ag cathode to investigate the possibility of all solution-processed PLEDs with PEO layer. The red, yellow, green and blue devices were fabricated with following structures:

R3: ITO/PEDOT:PSS (30 nm)/SPR-001 (80 nm)/Ag (100 nm)

R5: ITO/PEDOT:PSS (30 nm)/SPR-001 (80 nm)/PEO (0.5 mg/ml)/Ag (100 nm)

Y3: ITO/PEDOT:PSS (30 nm)/SPR-001 (80 nm)/Ag (100 nm)

Y5: ITO/PEDOT:PSS (30 nm)/SPR-001 (80 nm)/PEO (0.5 mg/ml)/Ag (100 nm)

G3: ITO/PEDOT:PSS (30 nm)/SPG-01T (80 nm)/Ag (100 nm)

G5: ITO/ PEDOT:PSS (30 nm)/SPG-01T (80 nm)/PEO (0.5 mg/ml)/Ag (100 nm)

B3: ITO/PEDOT:PSS (30 nm)/SPB-02T (80 nm)/Ag (100 nm)

B5: ITO/PEDOT:PSS (30 nm)/SPB-02T (80 nm)/PEO (0.5 mg/ml)/Ag (100 nm)

Unfortunately, the device performance was little increased in the PLEDs with PEO and Ag cathode compared to the devices without PEO layer. As shown in Figure 3.21, the operating voltage and luminance of PLEDs with PEO layer are higher and lower than those of devices without PEO layers. In

PEO layer mobile ions are not enough to enhance the electron injection and transport. So the operating voltage is increasing because of a thicker device thickness. And the efficiencies are similar or decreased with inserting the PEO layer shown in Figure 3.22. As can be seen in Figure 3.23, the normalized EL spectra of PLEDs with PEO layer are also similar to the devices without PEO layer.

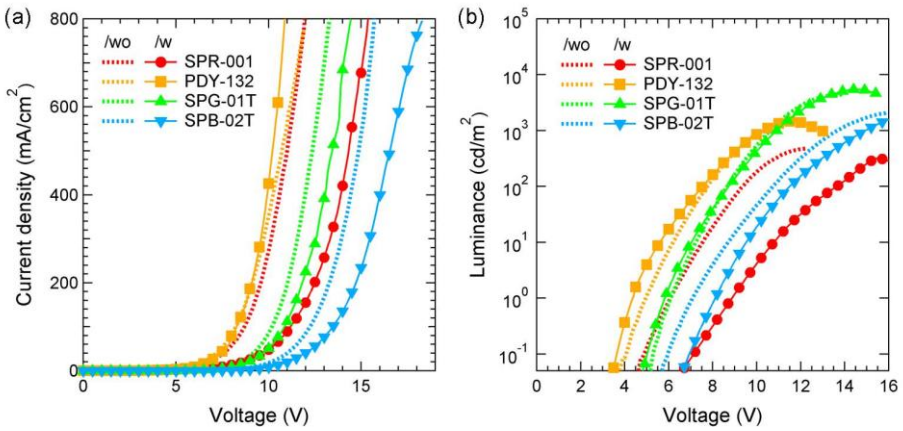

Figure 3.21 (a) J-V and (b) L-V characteristics of the red, yellow, green and blue PLEDs using Ag cathode with PEO layer.

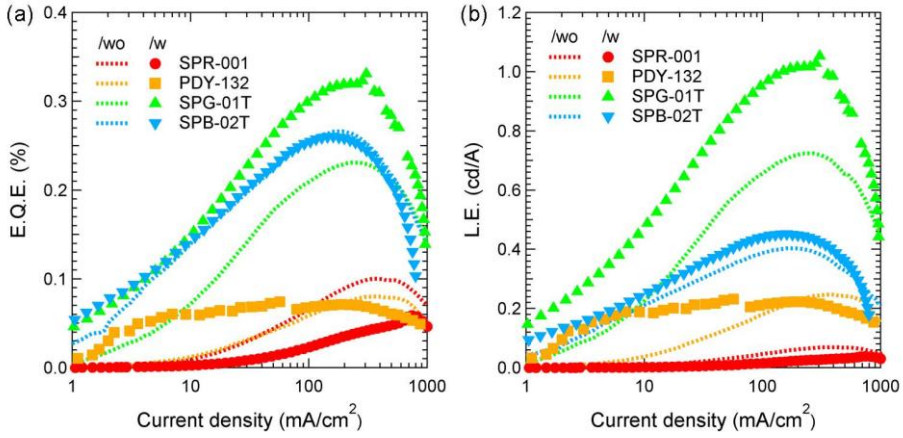

Figure 3.22 (a) EQE-J and (b) LE-J characteristics of the red, yellow, green and blue PLEDs using Ag cathode with PEO layer.

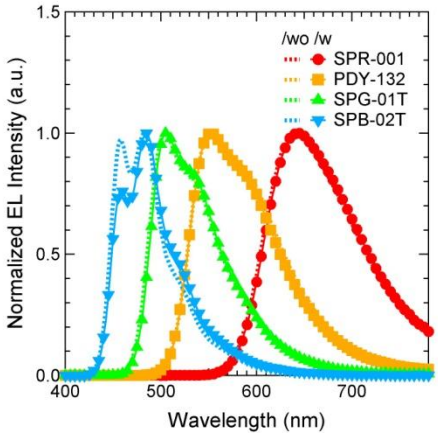

Figure 3.23 The normalized EL spectra at the same current density (J = 51 mA/cm^2) of the red, yellow, green and blue PLEDs using Ag cathode with PEO layer.

3.3.3 Device characteristics of PLEDs with PFN-P1 and Ag cathode

Recently, PFN series of conjugated polyelectrolyte is reported a lot [41,42,43]. So other conjugated polyelectrolyte, PFN-P1, is introduced in PLEDs with Ag cathode instead of PEO. The red, yellow, green and blue devices were fabricated with following structures:

R3: ITO/PEDOT:PSS (30 nm)/SPR-001 (80 nm)/Ag (100 nm)

R6: ITO/PEDOT:PSS (30 nm)/SPR-001 (80 nm)/PFN-P1 (2 mg/ml)/Ag (100 nm)

Y3: ITO/PEDOT:PSS (30 nm)/SPR-001 (80 nm)/Ag (100 nm)

Y6: ITO/PEDOT:PSS (30 nm)/SPR-001 (80 nm)/PFN-P1 (2 mg/ml)/Ag (100 nm)

G3: ITO/PEDOT:PSS (30 nm)/SPG-01T (80 nm)/Ag (100 nm)

G6: ITO/PEDOT:PSS (30 nm)/SPG-01T (80 nm)/PFN-P1 (2 mg/ml)/Ag (100 nm)

B3: ITO/PEDOT:PSS (30 nm)/SPB-02T (80 nm)/Ag (100 nm)

B6: ITO/PEDOT:PSS (30 nm)/SPB-02T (80 nm)/PFN-P1 (2 mg/ml)/Ag (100 nm)

The 2 mg of PFN-P1 is dissolved in 4 ml of methanol with 8 μl of acetic acid. Then PFN-P1 solution was spin-coated on top of the EL layer. Though introducing the PEO layer in PLEDs using Ag cathode was unsuccessful, the

device performances with PFN-P1 layer are dramatically increased compared to the devices without any layers between EML and Ag cathode. Similar to the case of KBH_4 doped 3TPYMB layer, the electron injection barrier still high, so the operating voltages of the devices are increased as shown in Figure 3.24(a). However dipole formation by PFN-P1 layer improved charge injection from cathode into light-emitting layers resulting in enhancement of the device performance.

Figure 3.25 shows the EQE-J and LE-J characteristics of the red, yellow, green and blue PLEDs using Ag cathode with PFN-P1. The maximum EQE of PLEDs using Ag cathode with PFN-P1 layer are 0.88, 1.46, 1.47 and 1.32% in red, yellow, green and blue PLEDs. And the maximum LE of PLEDs using Ag cathode with PFN-P1 layer are 0.57, 4.33, 4.72 and 2.46 cd/A in red, yellow, green and blue PLEDs. Those values are much higher than the efficiency of devices using just Ag electrode. (red: 0.1%, 0.070 cd/A, yellow: 0.08%, 0.25 cd/A, green: 0.23%, 0.72 cd/A and blue: 0.27%, 0.40 cd/A)

As shown in Figure 3.26, normalized EL spectra at the same current density (J = 51 mA/cm^2) of the red, yellow, green and blue PLEDs using Ag cathode with PFN-P1 layer are little red-shifted.

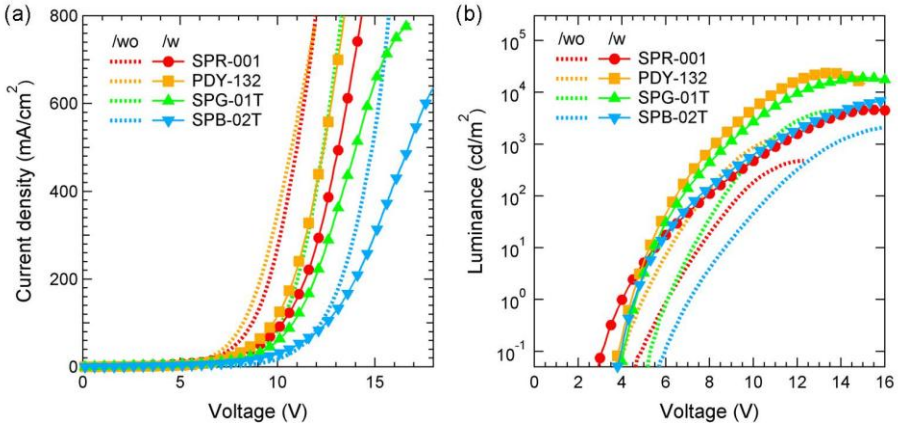

Figure 3.24 (a) J-V and (b) L-V characteristics of the red, yellow, green and blue PLEDs using Ag cathode with PFN-P1 layer.

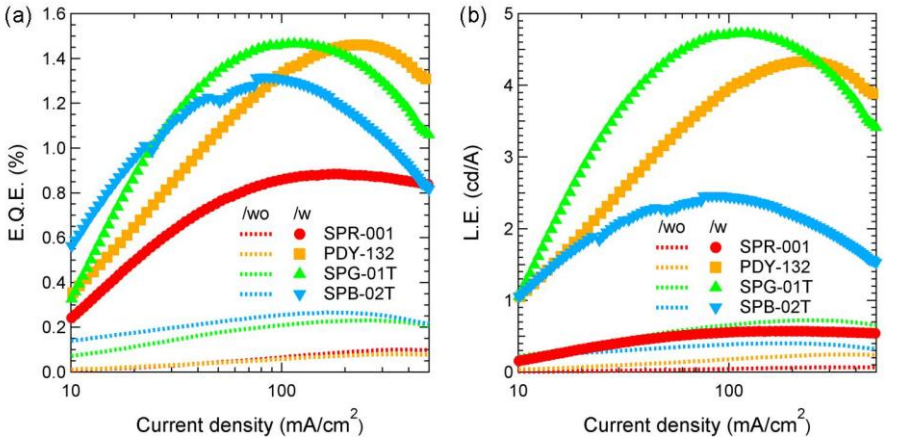

Figure 3.25 (a) EQE-J and (b) LE-J characteristics of the red, yellow, green and blue PLEDs using Ag cathode with PFN-P1 layer.

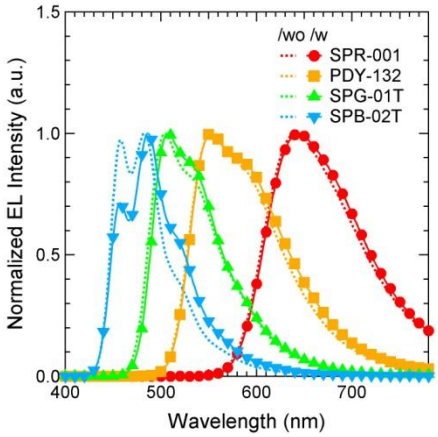

Figure 3.26 The normalized EL spectra at the same current density (J = 51 mA/cm^2) of the red, yellow, green and blue PLEDs using Ag cathode with PFN-P1 layer.

3.4 PLEDs with a Solution-processed cathode electrode

Although many efforts and significant improvements have been made on the development of solution-processed light-emitting materials, charge injection/transport materials and electrode materials, there is almost no attempt to combine these achievements together for fabricating all solution-processed OLEDs.

We fabricated successfully solution-processed PLEDs with a vacuum-evaporated Ag cathode electrode in above chapters. For better performance, we use the n-doped ETL and conjugated polyelectrolyte with Ag cathode; PLEDs with KBH_4 doped 3TPYMB show the best performances and PLEDs with PFN-P1 layer show the competitive performances compared with devices with n-doped ETL. Since these devices show good performances with vacuum-deposited Ag cathode, it is possible to fabricate the all solution-processed PLEDs having a good efficiency based on KBH_4 doped 3TPYMB or PFN-P1 layers. So we tried the fabrication of the all solution-processed PLEDs using KBH_4 doped 3TPYMB, because the PLEDs with KBH_4 doped 3TPYMB show the best performance.

3.4.1 Direct Ag printing on the PLEDs

As mentioned above, we used three kinks of Ag ink. Unfortunately, all inks dissolved KBH_4 doped 3TPYMB layer. The electron transport material,

3TPYMB, is soluble in almost the whole solvent such as methanol, toluene, chloroform, chlorobenzene, acetone, etc. So conjugated polyelectrolyte materials used in above chapter are introduced. However, PFN-P1 is also dissolved in the solvent of Ag ink and PEO is not effective in PLEDs with Ag cathode. Due to this solvent problem, the direct Ag printing on the PLEDs for fabrication of all solution-processed PLEDs is impossible. The solvents and specific properties of three commercial Ag inks are summarized in Table 3.4.

Table 3.4 Ag ink specification

Company	InkTec	ANP	Sigma-Aldrich
Iink type	precursor	nanoparticle	nanoparticle
Concentration	15 wt%	30–35 wt%	20 wt%
Solvents	Toluene Methanol Anisole	Triethylene glycol monoethyl ether (TGME)	Ethanol Ethanediol
Viscosity (cps)	9–15	10–17	11.6–13
Surface tension (dynes/cm)	30–32	35–38	28–31
Particle size	-	40–60 nm	< 150 nm

3.4.2 Lamination of printed Ag electrode on PDMS

Because the n-doped ETL and conjugated polyelectrolyte are dissolved by the solvent of Ag ink as mentioned above, we tried lamination of printed Ag electrode on poly(dimethylsiloxane) (PDMS). The PDMS mold was prepared by curing the mixture of Sylgard 184 A and B (with a volume ratio of 10:1). Ag electrode is deposited by ink-jet printing on prepared PDMS, and then dried on hotplate at 120 ℃ for 10 min. After that process, Ag electrode on PDMS is laminated onto a pre-fabricated PLED. Figure 3.27 shows a schematic diagram of Ag printing on PDMS and lamination onto PLEDs.

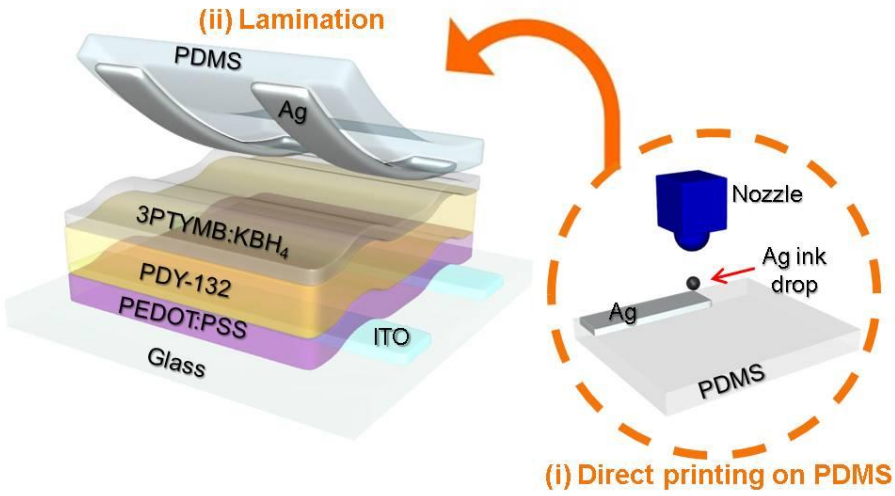

Figure 3.27 A schematic diagram of Ag printing on PDMS and lamination onto a pre-fabricated PLED.

Originally, PDMS has a rough surface. In drying printed Ag on PDMS, coefficient of expansion is different between PDMS and Ag; the roughness is increased. Due to this problem, the adhesion between pre-fabricated PLED and printed Ag electrode on PDMS is bad and device performance is poor. The current density-voltage-luminance (J-V-L) characteristics of all solution-processed PLED with laminated Ag printed electrode is shown in Figure 3.28. And Figure 3.29(a) shows EQE-J characteristics of this device. The operating voltage is much higher than the PLEDs with vacuum-evaporated Ag cathode. The maximum EQE is 0.0004%; this value is also very low. The normalized EL spectrum at 51 mA/cm^2 is similar with the devices with vacuum-evaporated Ag cathode.

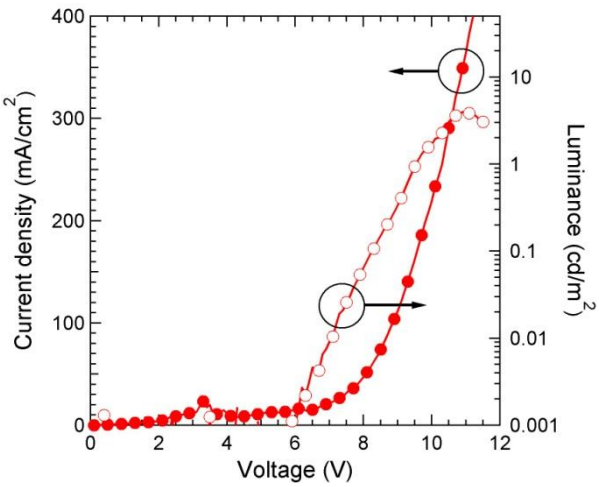

Figure 3.28 The J-V-L characteristics of all solution-processed PLED with laminated Ag printed electrode.

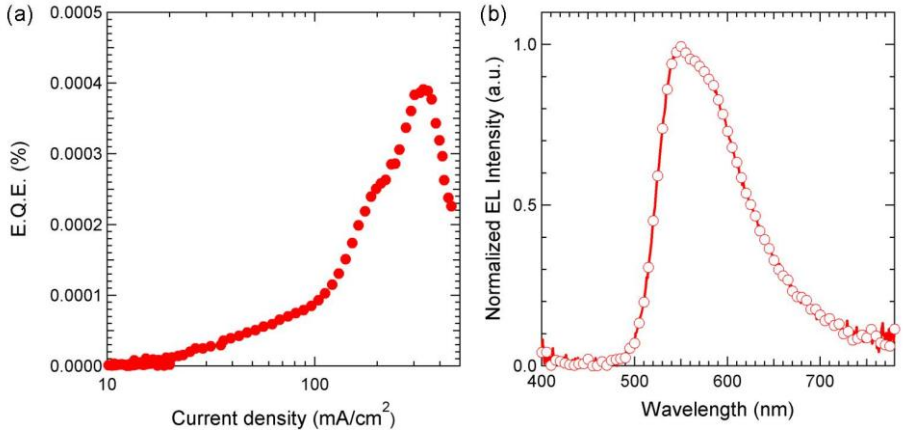

Figure 3.29 (a) EQE-J characteristics and (b) normalized EL spectrum at 51 mA/cm^2 of all solution-processed PLED with laminated Ag printed electrode.

Chapter 4. Solution-processed Polymer Light-Emitting Diodes with an Inverted Device Structure

Since most of PLEDs with a conventional structure were fabricated using PEDOT:PSS as HIL and HTL, ETL or EIL is a major challenge in fabrication of solution-processed PLEDs to achieve high efficient devices. However, in case of solution-processed PLEDs with an inverted device structure, a hole injection is also important issues as well as an electron injection. So we fabricate PLEDs with self-assembled monolayer (SAM) or conjugated polyelectrolyte for improving an electron injection. After that, we introduce several HILs such as MoO_3 nanoparticles, PEDOT:PSS and sol-gel V_2O_5 for increasing a hole injection efficiency.

4.1 Solution-processed inverted PLEDs with a self-assembled monolayer

In fabrication of inverted PLEDs, metal oxide such as ZnO, titanium dioxide (TiO_2) is used for electron injection layer. However, light-emitting polymers are cannot be deposited on that layer due to the mismatch between the work function of metal oxide and LUMO of polymers. Therefore, lowering the work function of metal oxide is an important issue. One approach is to

improve the electron injection ability using the SAM treatment. SAM can adjust the work function by producing a permanent dipole moment at interface. Using this concept, many studies have been reported. In this thesis, we treat benzoic acid-based SAM on the ZnO layer for improving electron injection ability and investigate the device performance.

4.1.1 Preparation of self-assembled monolayers

We used three benzoic acid-based self-assembled materials which was purchased from Merk; 4-Methoxybenzoic acid (BA-OCH_3), 4-Cyanobenzoic acid (BA-CN) and 4-(Trifluoromethyl)benzoic acid (BA-CF_3). The self-assembled molecules were deposited onto the ZnO layer by using a two-step spin-coating process. First, 1 mM of the molecules in ethanol was spin-coated onto the ZnO film, and a monolayer of the molecules was formed through chemical bonding between carboxylic acid and ZnO. To remove physically absorbed molecules, a second spin-coating using pure ethanol was applied. The formation of the SAMs was confirmed by results from contact angle measurements after surface modification. (see Figure 4.1)

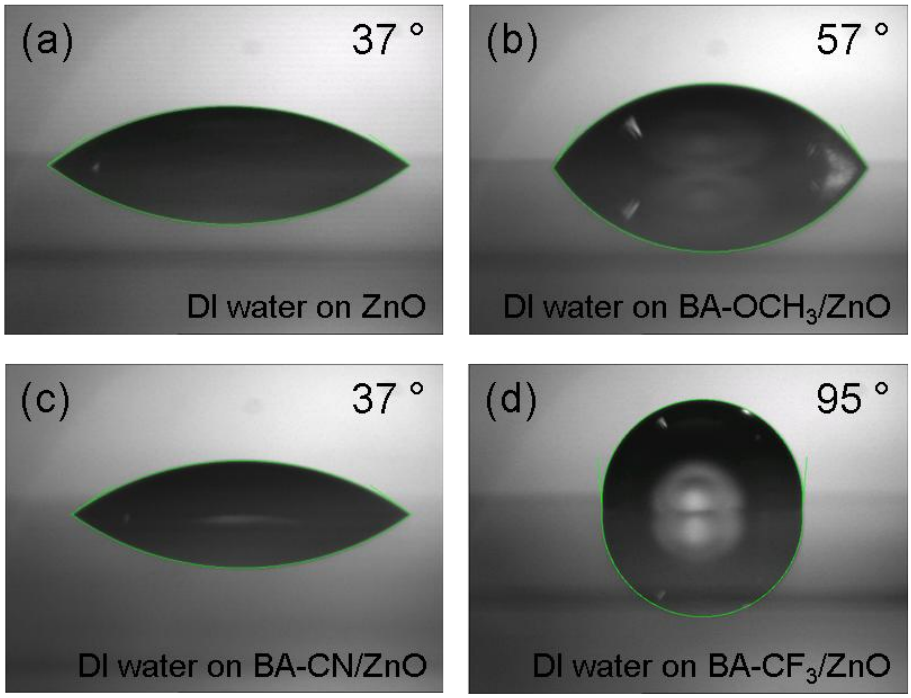

Figure 4.1 The liquid drop images of a polar solvent (DI water) on (a) the ZnO layer and (b,c,d) various SAM coated onto ZnO layer to measure the contact angles.

4.1.2 Device characteristics of solution-processed PLEDs with various self-assembled monolayers

The device structure of the PLEDs with SAM is shown in Figure 4.2; ITO on glass/ZnO (40 nm)/SAM/PDY-132 (80 nm)/FSO-100 doped PEDOT:PSS (1 wt%, 60 nm)/Ag (100 nm). In the device, Ag electrode is deposited by vacuum evaporation. SAM forms an interfacial dipole which influences the charge injection barrier. So the dipole moment and direction are important factors. Shown in Figure 4.3, The gas-phase dipole moment of the benzoic

acid derivatives increased in order when substituted with –OCH3 (-2.45 D) < –CF3 (1.88 D) < –CN (3.57 D).

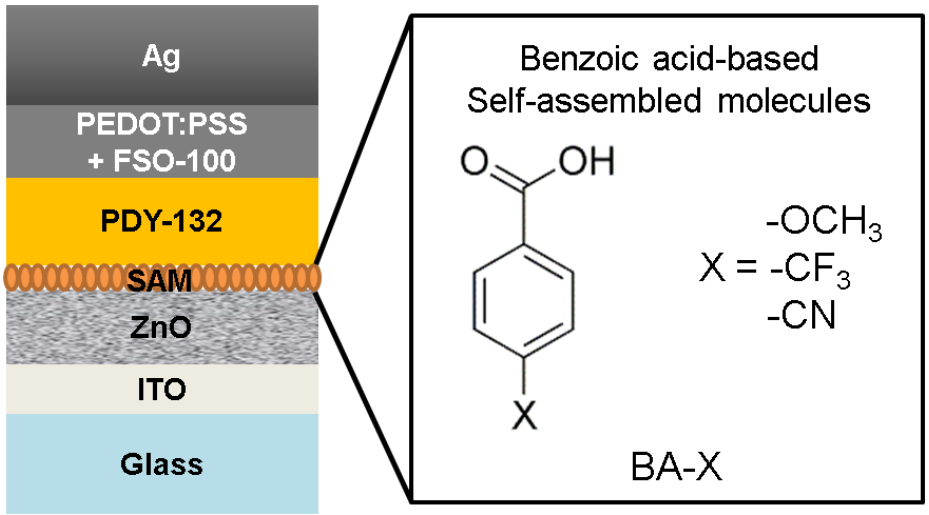

Figure 4.2 Device architecture of the PLEDs with self-assembled monolayer and the chemical structures of the self-assembling molecules used in this study.

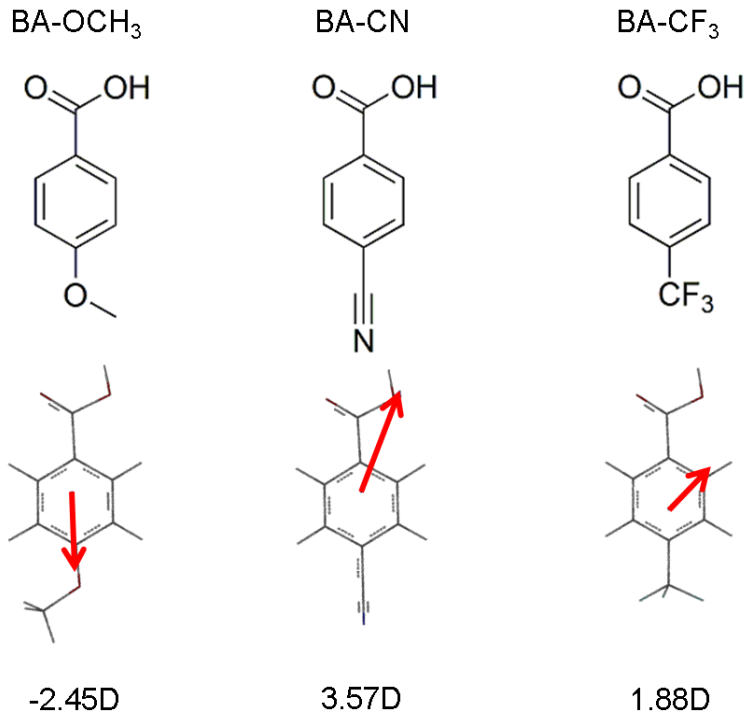

Figure 4.3 The gas-phase dipole moment of the benzoic acid derivatives.

Based on the calculated dipole moment of SAMs, we guess the formation of dipole in the interface between ZnO layer and EML. Shown in Figure 4.4, electron injection barrier is very high about ~1.3 eV. In case of BA-OCH_3 SAM, the interfacial dipole directed away from the ZnO layer decrease the electron injection barrier. On the other hand, BA-CN and BA-CF_3 SAMs form the interfacial dipole directed towards the ZnO layer and they increase the electron injection barrier. For investigating the effect of SAMs in the real devices, we fabricated the PLEDs with or without three kinds of SAMs between ZnO layer and EML shown in Figure 4.2.

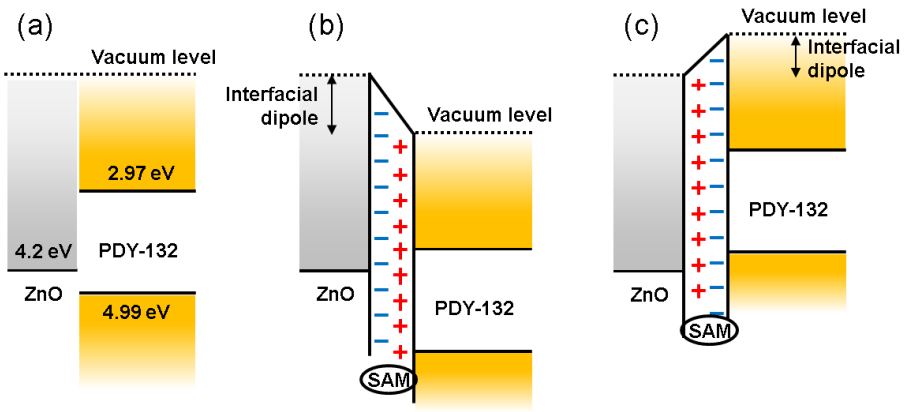

Figure 4.4 Schematic illustration of the energy level diagram with (a) a ZnO/metal bilayer cathode, (b) a ZnO/SAM/metal cathode with an interfacial dipole directed away from the metal surface and (c) a ZnO/SAM/metal cathode with an interfacial dipole directed towards the metal surface.

Figure 4.5 shows J-V and L-V characteristics of the devices with or without various SAMs. Inevitably, the PLED with BA-OCH_3 SAM shows better performances than the PLED without any SAMs. And the PLED with BA-CN and BA-CF_3 SAMs show worse performances than the PLED without any SAMs. Because the electron injection barrier between ZnO layer and EML is so high (~1.3 eV), EQE of the PLED with BA-OCH_3 is still low.

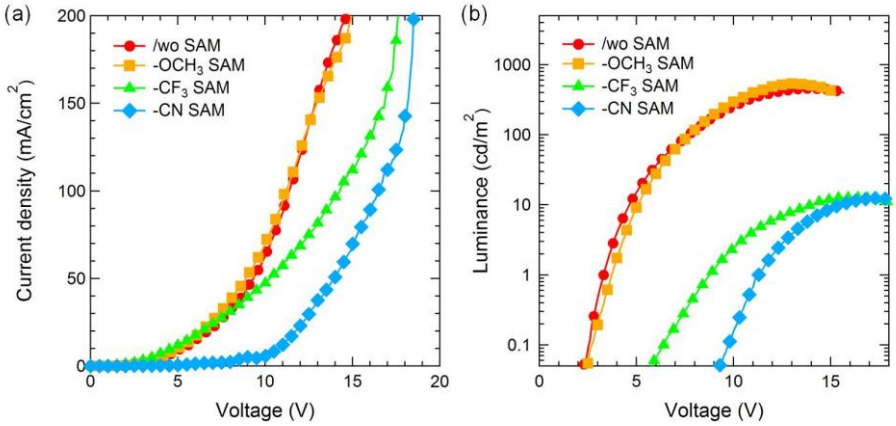

Figure 4.5 (a) J-V and (b) L-V characteristics of the PLEDs with various SAM layers.

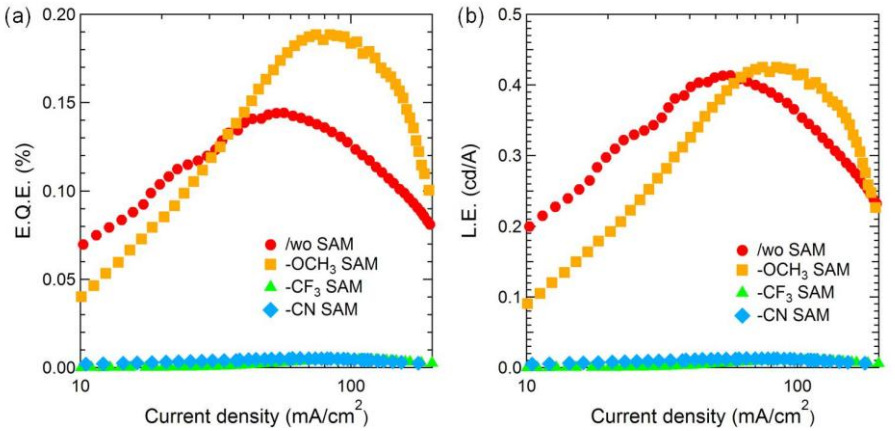

Figure 4.6 (a) EQE-J and (b) LE-J characteristics of the PLEDs with various SAM layers.

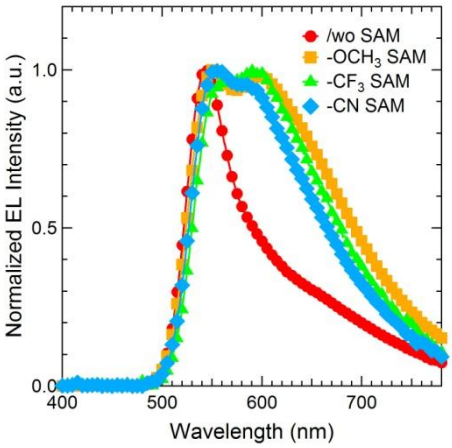

Figure 4.7 The normalized EL spectra at the same current density (J = 51 mA/cm^2) of the PLEDs with various SAM layers.

4.2 Solution-processed inverted PLEDs with conjugated polyelectrolyte

Though BA-OCH_3 of self-assembled monolayer forms the interfacial dipole directed away from the ZnO layer and decreases the electron injection barrier, the effect is low. For better performances, conjugated polyelectrolyte, PFN-P1, is the better way used in the previous section. In conventional structured PLEDs, we used toluene for dissolving light-emitting polymers. However, the PFN-P1 layer is diluted by toluene. So we used chlorobenzene for the solvent.

4.2.1 Optimization of device characteristics depending on PFN-P1 layer thickness for electron injection

The PLEDs had a configuration of ITO/ZnO (40 nm)/PFN-P1 (0.5-3 mg/ml)/PDY-132 (80 nm)/MoO_3 (10 nm)/Ag (100 nm). All layers are deposited by spin-coating except MoO_3 layer and Ag electrode. These two layers are deposited using vacuum deposition systems.

Figure 4.8 shows J-V and L-V characteristics of the devices with a various concentrations of PFN-P1. As can be seen from Figure 4.8(b), the turn-on voltages at 0.1 cd/m^2 are 1.6–1.7 V for the devices with PFN-P1 layer. The insertion of the PFN-P1 layer helped to reduce the turn-on voltage by more than 0.7 V compared device without PFN-P1 layer. The maximum luminance is also improved. The maximum luminance of the devices with

PFN-P1 layer are 22,600, 37,000, 26,800, 29,000 and 27,300 cd/m^2 for the concentrations of 0.5, 1, 1.5, 2 and 3 mg/ml. All devices with PFN-P1 shows 7–12 times higher luminance than the device without PFN-P1 layer.

As shown in Figure 4.9(a), EQE and LE of the device increases dramatically with PFN-P1 layer. All devices with various PFN-P1 concentrations show higher EQE than the PLEDs without PFN-P1 layer. Especially, the PLED with PFN-P1 layer of 2 mg/ml concentration have EQE of 1.06%. This value is 70% higher than the EQE of PLED without PFN-P1 layer. These results indicate that the PFN-P1 layer lowering an electron injection barrier and transport of electrons become well; electron-hole balance becomes to be improved. As shown in Figure 4.10, the EL spectra normalized at the main emission peak (587 nm) at a current density of 51 mA/cm^2 have no significant difference by introducing PFN-P1 layers. We summarize the performance of PLEDs with PFN-P1 layers in Table 4.1.

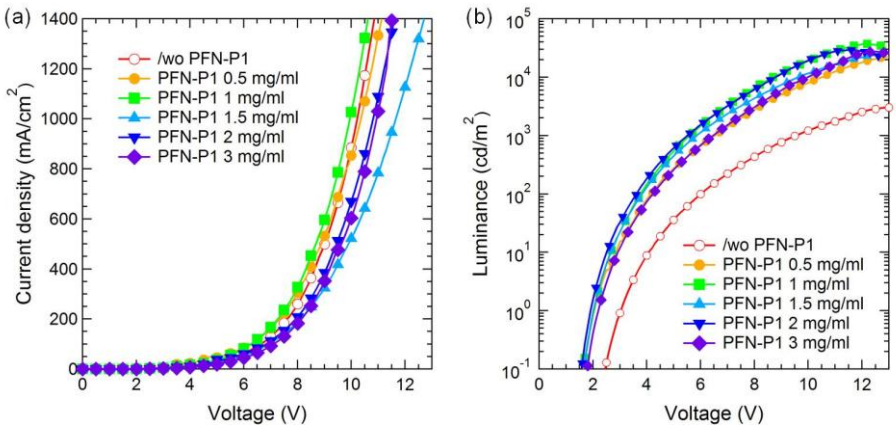

Figure 4.8 (a) J-V and (b) L-V characteristics of the PLEDs with various PFN-P1 concentrations.

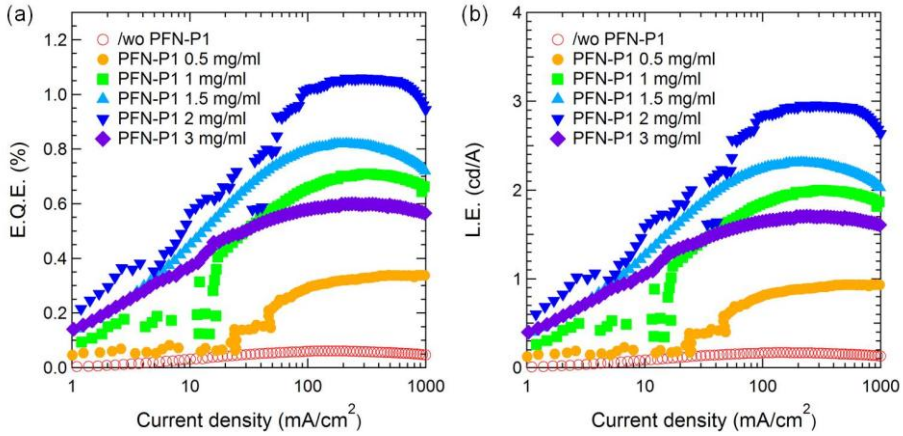

Figure 4.9 (a) EQE-J and (b) LE-J characteristics of the PLEDs with various PFN-P1 concentrations.

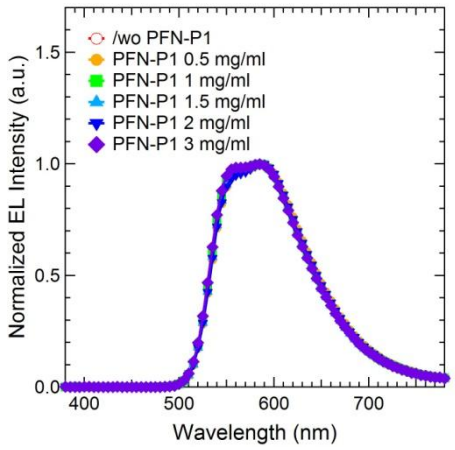

Figure 4.10 The normalized EL spectra at the same current density (J = 51 mA/cm^2) of the PLEDs with various PFN-P1 concentrations.

Table 4.1 The device performances of OLEDs with or without PFN-P1 layer.

	Max. L (cd/m^2)	Max. E.Q.E (%)	Max. L.E. (cd/A)	EL λ_{max} (nm)
Without PFN-P1	3,000	0.62	0.17	587
PFN-P1 0.5 mg/ml	22,600	0.34	0.94	587
PFN-P1 1 mg/ml	37,000	0.71	2.00	587
PFN-P1 1.5 mg/ml	26,800	0.82	2.31	587
PFN-P1 2 mg/ml	29,000	1.06	2.96	587
PFN-P1 3 mg/ml	27,300	0.60	1.71	584

4.2.2 Device characteristics of red, yellow, green and blue PLEDs with a PFN-P1 layer

The red, green and blue devices with PFN-P1 layer were also fabricated with following structures:

Red: ITO/ZnO (40 nm)/PFN-P1 (2 mg/ml)/SPR-001 (80 nm)/MoO_3 (10 nm)/Ag (100 nm).
Green: ITO/ZnO (40 nm)/PFN-P1 (2 mg/ml)/SPG-01T (80 nm)/MoO_3 (10 nm)/Ag (100 nm).
Blue: ITO/ZnO (40 nm)/PFN-P1 (2 mg/ml)/SPB-02T (80 nm)/MoO_3 (10 nm)/Ag (100 nm).

In these devices, MoO_3 layer and Ag electrode are deposited by thermal depositions. The device performances with PFN-P1 layer are dramatically increased in the red, yellow and green devices with PFN-P1 layer. Figure 4.11 shows J-V and L-V characteristics of the red, yellow, green and blue devices with a PFN-P1 layer. As can be seen from Figure 4.11(b), the turn-on voltages at 0.1 cd/m^2 are 1.8, 1.6, 2.2 and 2.6 V for the red, yellow, green and blue devices with PFN-P1 layer, respectively. The insertion of the PFN-P1 layer helped to reduce the turn-on voltage by 0.7, 0.8, 1.1 and 1.9 V, respectively, compared to red, yellow, green and blue devices without PFN-P1 layer. The maximum luminance is also improved. The maximum luminance of the devices with PFN-P1 layer are 6,400, 29,000, 29,000 and 13,500 cd/m^2 for the

red, yellow, green and blue devices with PFN-P1 layer. All devices with PFN-P1 show higher luminance than the device without PFN-P1 layer. (red: 400 cd/m^2, yellow: 3,000 cd/m^2, green: 2,500 cd/m^2 and blue: 30 cd/m^2)

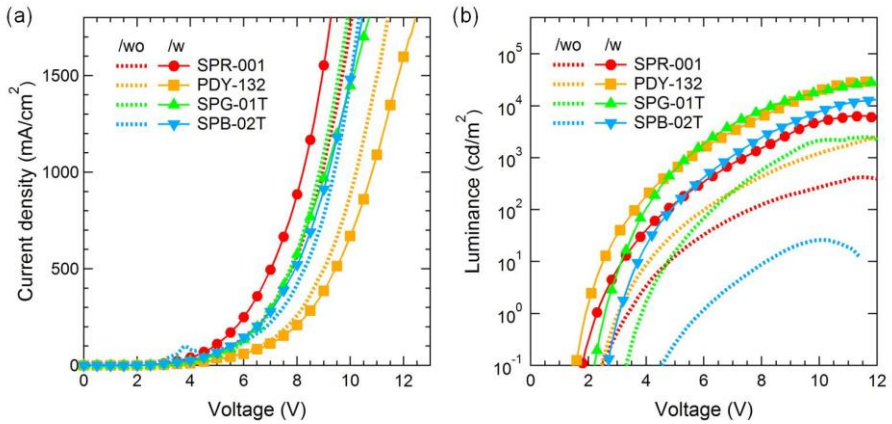

Figure 4.11 (a) J-V and (b) L-V characteristics of the red, yellow, green and blue PLEDs with or without a PFN-P1 layer.

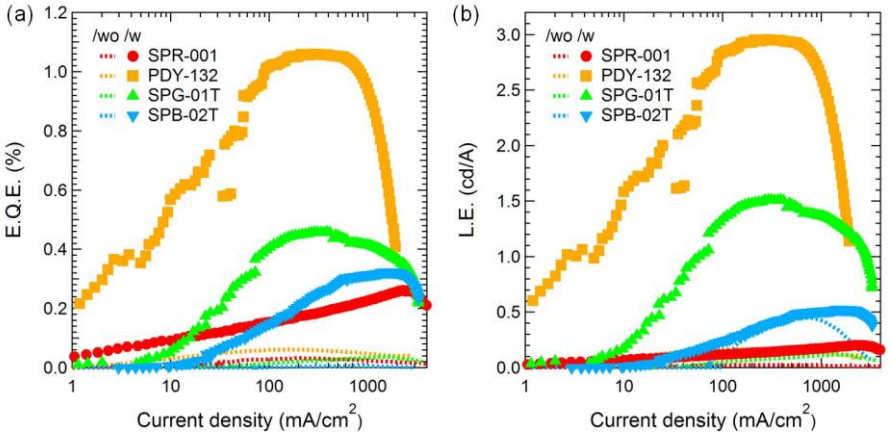

Figure 4.12 (a) EQE-J and (b) LE-J characteristics of the red, yellow, green and blue PLEDs with or without a PFN-P1 layer.

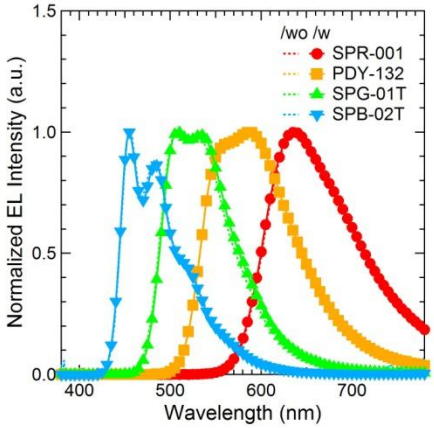

Figure 4.13 The normalized EL spectra at the same current density (J = 51 mA/cm^2) of the red, yellow, green and blue PLEDs with or without a PFN-P1 layer.

As shown in Figure 4.12, EQE and LE of the device are improved dramatically by inserting PFN-P1 layer. All devices with PFN-P1 layer show higher efficiency than the PLEDs without PFN-P1 layer. The maximum EQE of the devices with PFN-P1 layer are 0.26, 1.06, 0.46 and 0.32% for the red, yellow, green and blue devices with PFN-P1 layer. And the maximum LE of the devices with PFN-P1 layer are 0.20, 2.96, 1.51 and 0.52 cd/A for the red, yellow, green and blue devices with PFN-P1 layer. All devices with PFN-P1 show higher EQE and LE than the device without PFN-P1 layer. (red: 0.03%, 0.025 cd/A, yellow: 0.062%, 0.17 cd/A, green: 0.04%, 0.12 cd/A and blue: 0.006%, 0.45 cd/A) Though the EQE and LE of the devices are highly improved, these values were lower than the EQE and LE of the conventional PLEDs with PFN-P1 layer. These differences come from the structure

difference as well as the aggregation differences of polymers by using a different solvent.

As shown in Figure 4.13, the EL spectra normalized at the main emission peak at a current density of 51 mA/cm^2 have no difference by introducing PFN-P1 layers. We summarize the performance of PLEDs with PFN-P1 layers in Table 4.2.

Table 4.2 The device performances of red, green and blue OLEDs without or with PFN-P1 layer.

	Red OLED		Green OLED		Blue OLED	
	/wo	/w	/w	/w	/wo	/w
Max. Luminance (cd/m^2)	400	6,400	2,500	29,000	30	13,500
Max. EQE (%)	0.03	0.26	0.04	0.46	0.006	0.32
Max. LE (cd/A)	0.025	0.20	0.12	1.51	0.45	0.52
EL λ_{max} (nm)	637	637	508	508	455	455

4.3 Inverted PLEDs with various solution-processed HILs

In this part, we fabricate inverted PLEDs with solution processed HILs; PEDOT:PSS, MoO_3 nanoparticles and sol-gel V_2O_5 and investigate the device performances.

4.3.1 Device characteristics of solution-processed inverted PLEDs with MoO_3 nanoparticles

The MoO_3 nanoparticles (purchased from Nanograde GmbH) we used have a 5 wt% of surfactant stabilized by an undisclosed block copolymer. In previous research by other group, they treated O_2 plasma (1 min, 200 W, 0.2 Torr, gas flow ~40 sccm) to remove the dispersing agent [17]. However, light-emitting polymers are located under solution-processed HIL in our inverted structure of PLEDs. So oxygen plasma treatment which destroy underlying layers cannot be adopted. To solve this problem, we used two-step spin-coating process. First, MoO_3 nanoparticles in ethanol was spin-coated onto the EML, and then dried at hotplate at 80 ℃ for 30 min. To remove surfactant of MoO_3, a second spin-coating using pure n-hexane was applied. (we called solvent washing, SW) For investigating the effect of solvent washing, we fabricated the PLEDs with or without solvent washing. The devices with MoO_3 nanoparticles were fabricated with following structures: ITO/ZnO (40

nm)/PFN-P1 (2 mg/ml)/PDY-132 (80 nm)/solution-processed MoO_3 (0.1-1 wt%)/with or without solvent washing/Ag (100 nm). All layers are deposited by spin-coating except vacuum-evaporated Ag cathode. For comparison, the PLED with vacuum-deposited MoO_3/Ag layers is fabricated.

Figure 4.14 shows J-V and L-V characteristics of the devices with MoO_3 nanoparticles and solvent washing. In Figure 4.14(a), the operating voltages are increased by increasing the concentrations of MoO_3 nanoparticles. But the operating voltage is very high than that of the PLEDs with vacuum-evaporated MoO_3. Maybe the reason is surfactant of MoO_3 nanoparticles which disturb flowing of charges. As solvent washing is applied to coated MoO_3 layer, the operating voltage is decreased in the device with 0.5 wt% of MoO_3. It means the solvent washing is working for removing the surfactant. However, in 1 wt% of MoO_3, the thickness of coated MoO_3 layer is thicker and the solvent washing is not working. Though the operating voltage is decreased by solvent washing, it is still high than that of the device with vacuum-evaporated MoO_3 layer. In previous research in other lab, solution-processed MoO_3 films provide the same hole-injection efficiency as thermally evaporated MoO_3. It means solvent washing is working, but surfactant is not removed at all. This problem influences an operating voltage, luminance and efficiency.

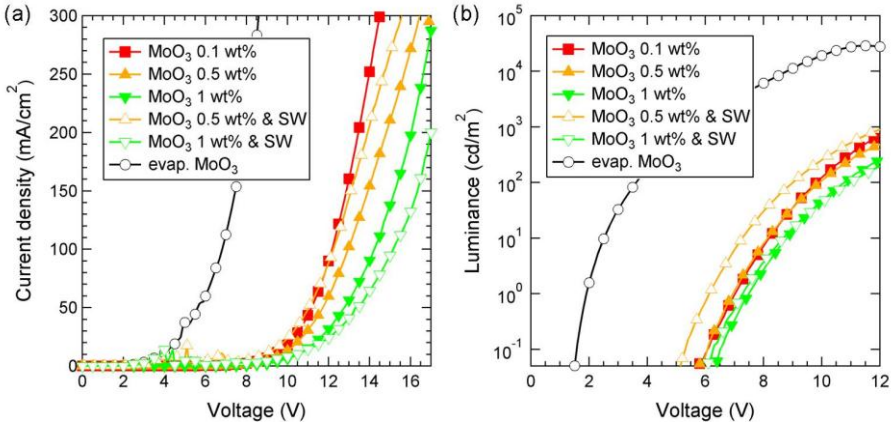

Figure 4.14 (a) J-V and (b) L-V characteristics of the PLEDs with various MoO_3 nanoparticles concentrations and a solvent washing.

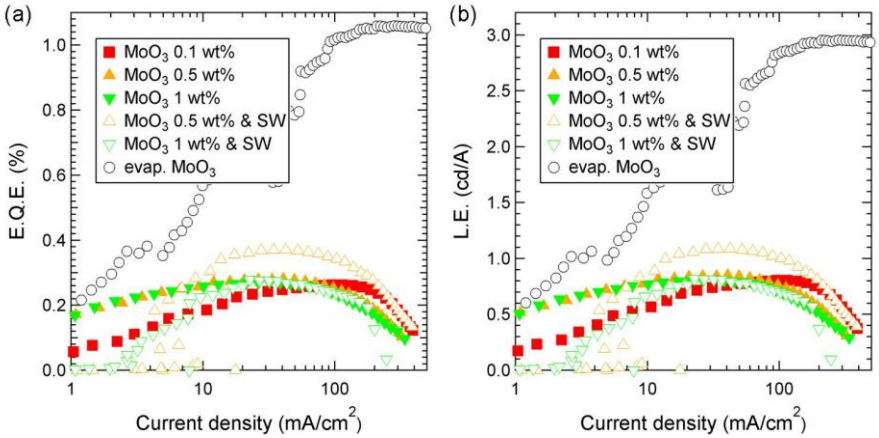

Figure 4.15 (a) EQE-J and (b) LE-J characteristics of the PLEDs with various MoO_3 nanoparticles concentrations and a solvent washing.

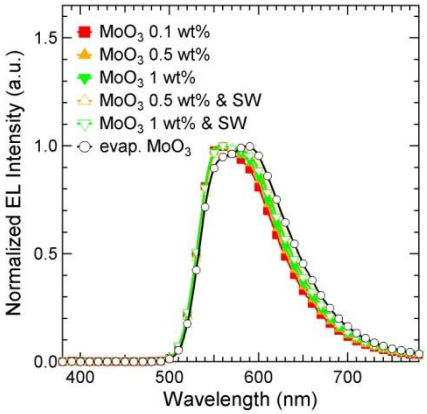

Figure 4.16 The normalized EL spectra at the same current density (J = 51 mA/cm^2) of the PLEDs with various MoO_3 nanoparticles concentrations and a solvent washing.

As shown in Figure 4.14(b), the luminance is very low than that of device with vacuum-evaporated MoO_3 regardless of solvent washing. Figure 4.15 shows EQE-J and LE-J characteristics of PLEDs with various MoO_3 nanoparticles concentrations. The maximum EQE and LE of the device with spin-coated MoO_3 is also very low than that of device with vacuum-evaporated MoO_3 regardless of solvent washing. These results indicate that the remained surfactant disturb an electron injection and transport; electron-hole balance becomes to be worse. As shown in Figure 4.16, the maximum peak wavelength is changed in the device with MoO_3 nanoparticles. It is because the recombination zone is shifted by disturbing electron transportation from remained surfactant.

4.3.2 Device characteristics of solution-processed inverted PLEDs with PEDOT:PSS

PEDOT:PSS is one of the most commonly used hole injection materials due to its high conductivity, good hole injection for solution process. However, in our inverted PLED case, PEDOT:PSS cannot be spin-coated on the hydrophobic layer of light-emitting polymers. For this problem, we add 1 wt% of surfactant (FSO-100) in PEDOT:PSS to aid wetting. The devices with PEDOT:PSS HIL were fabricated with following structures: ITO/ZnO (40 nm)/PFN-P1 (2 mg/ml)/PDY-132 (80 nm)/FSO-100 doped PEDOT:PSS (1 wt%, 60 nm)/Ag (100 nm). All layers are deposited by spin-coating except Ag cathode. For comparison, the PLED with vacuum-deposited MoO_3/Ag layers is also fabricated.

Figure 4.17 shows J-V and L-V characteristics of the devices with PEDOT:PSS layer. In Figure 4.17(a), the operating voltages are increased in the device with PEDOT:PSS layer. The thickness of PEDOT:PSS layer was about 60 nm. It is thicker than the thermally evaporated MoO_3 of 10 nm. And it is known that a conductivity of PEDOT:PSS with surfactant is decreased. These reasons make the device performances poor.

As shown in Figure 4.17(b) and Figure 4.18, the luminance and maximum efficiency are very low than that of device with vacuum-evaporated MoO_3. These results indicate that the PEDOT:PSS with FSO-100 has lower electron injection efficiency than vacuum-evaporated MoO_3. As shown in

Figure 4.19, the overall shape of EL spectra at current density of 51 mA/cm^2 is changed in the device with PEDOT:PSS layer.

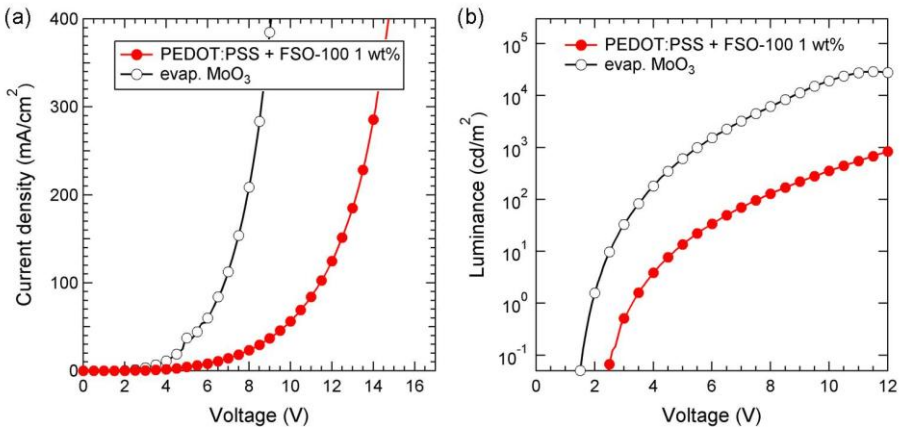

Figure 4.17 (a) J-V and (b) L-V characteristics of the PLEDs with PEDOT:PSS layer and vacuum-evaporated MoO_3 layer.

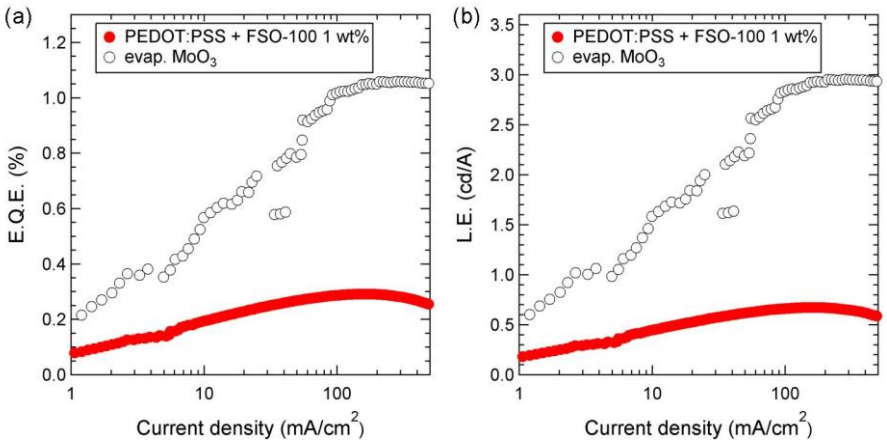

Figure 4.18 (a) EQE-J and (b) LE-J characteristics of the PLEDs with PEDOT:PSS layer and vacuum-evaporated MoO_3 layer.

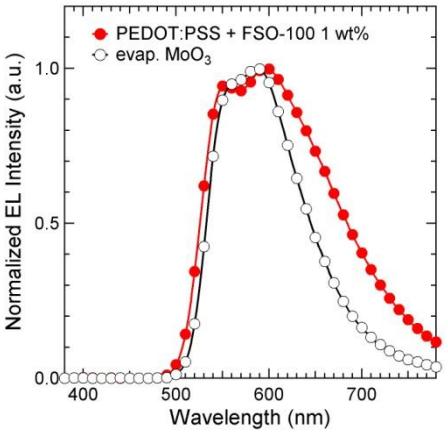

Figure 4.19 The normalized EL spectra at the same current density (J = 51 mA/cm^2) of the PLEDs with PEDOT:PSS layer and vacuum-evaporated MoO_3 layer.

4.3.3 Device characteristics of solution-processed inverted PLEDs with sol-gel V_2O_5

Recently, Zilberberg *et al.* used sol-gel derived V_2O_5 layers in inverted organic solar cells [18]. In their research, sol-gel V_2O_5 layers show high work function (5.6 eV), smooth surface and air stability. Furthermore, additional treatments does not required for pure V_2O_5 layers. Because of these advantages sol-gel V_2O_5 layers are attractive HIL for the solution-processed PLEDs. So we fabricate the PLEDs with various V_2O_5 concentrations and investigate the device performances. The V_2O_5 layer was spin-coated from isopropanol solution of vanadium(V) oxitriisopropoxide (purchased from Alfa Aesar) at 1:100, 1:150 and 1:200 vol. ratio. The layers were subsequently stored at ambient air for 1 hour for hydrolysis. The devices with V_2O_5 HIL

were fabricated with following structures: ITO/ZnO (40 nm)/PFN-P1 (2 mg/ml)/PDY-132 (80 nm)/V_2O_5 (1:100, 1:150 and 1:200 vol. ratio)/Ag (100 nm). All layers are deposited by spin-coating except Ag cathode. For comparison, the PLED with vacuum-deposited MoO_3/Ag layers is also fabricated.

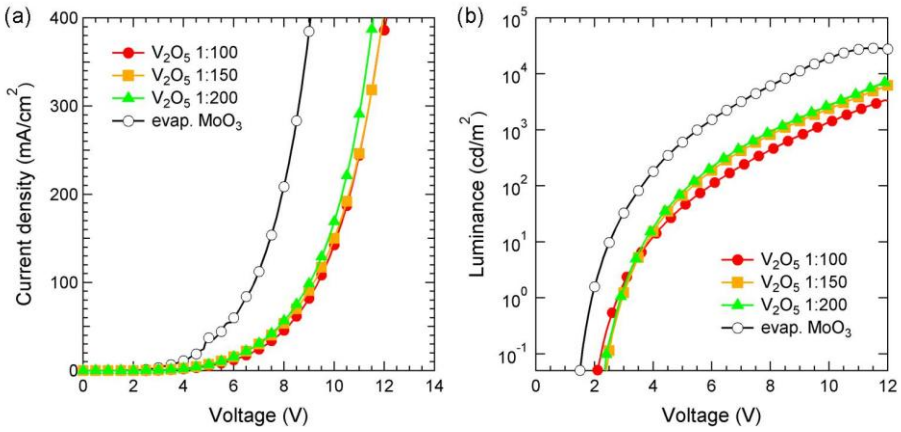

Figure 4.20 (a) J-V and (b) L-V characteristics of the PLEDs with sol-gel V_2O_5 and vacuum-evaporated MoO_3 layer.

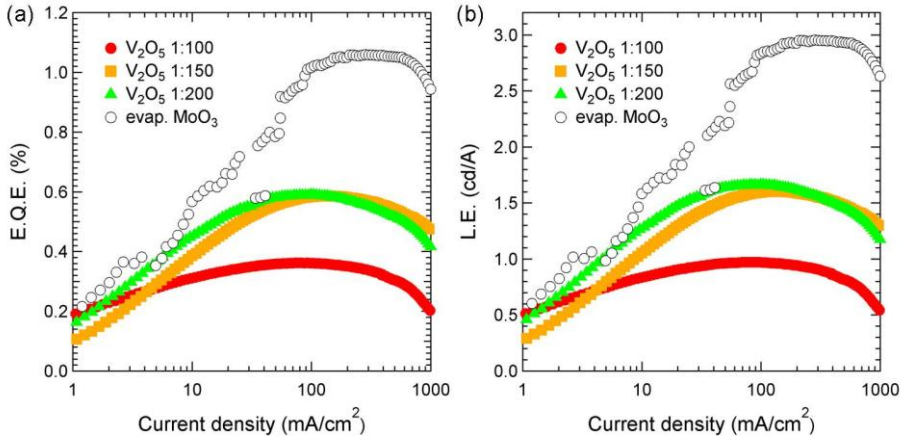

Figure 4.21 (a) EQE-J and (b) LE-J characteristics of the PLEDs with sol-gel V_2O_5 and vacuum-evaporated MoO_3 layer.

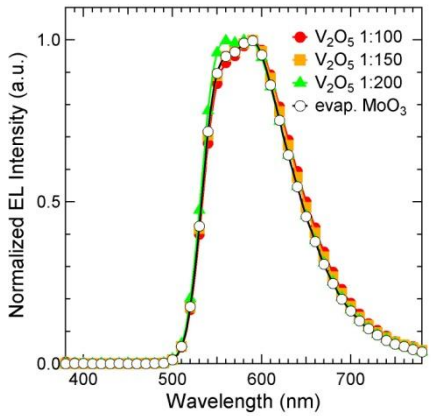

Figure 4.22 The normalized EL spectra at the same current density (J = 51 mA/cm^2) of the PLEDs with sol-gel V_2O_5 and vacuum-evaporated MoO_3 layer.

As shown in Figure 4.20, the operating voltage is decreasing and luminance is increasing as decreasing the V_2O_5 ratio. It means a thin V_2O_5 layer is more effective to increase an electron injection. In maximum EQE

and LE, thin V_2O_5 works efficiently as shown in Figure 4.21. However, all values of the performance with V_2O_5 is lower than that of device with vacuum-evaporated MoO_3. These results indicate that the V_2O_5 has lower electron injection efficiency than vacuum-evaporated MoO_3. As shown in Figure 4.22, the overall shape of EL spectra at the same current density (J = 51 mA/cm^2) is similar in the devices with V_2O_5 layers.

4.3.4 Comparison to device performances of solution-processed inverted PLEDs with various HILs

We fabricated inverted PLEDs with solution processed HILs; PEDOT:PSS, MoO_3 nanoparticles and sol-gel V_2O_5. As can be seen in Figure 4.23, the PLED with V_2O_5 layer shows better performance than the devices with other solution-processed HILs. However, it is still worse performance compare to the device with vacuum-evaporated MoO_3.

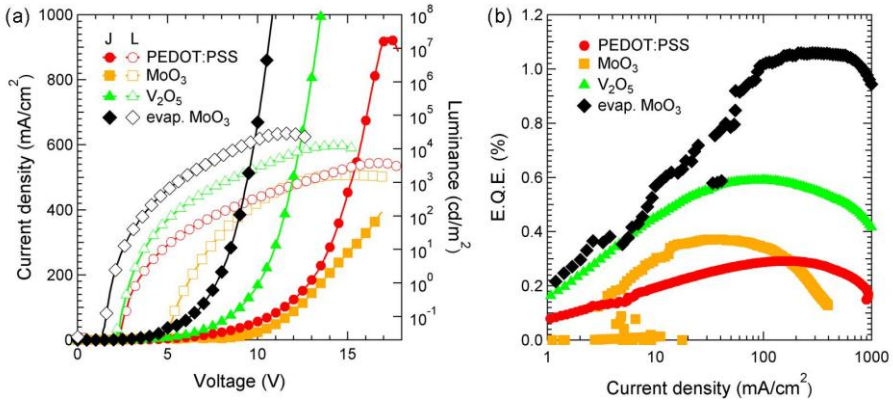

Figure 4.23 (a) J-V-L and (b) EQE-J characteristics of the PLEDs with various HILs.

4.4 Inverted PLEDs with a Solution-processed cathode electrode

In previous chapter, we fabricated all solution-processed PLEDs with a conventional device structure. For developing more efficient all solution-processed PLEDs, we fabricate this device with inverted device structure using PFN-P1 layer, sol-gel V_2O_5 and ink-jet printed Ag cathode. When we deposit Ag electrode using Ag ink purchased from InkTec, sintering cannot be done. So Ag electrode is not formed exactly and the device is not working.

When we use the Ag nanoparticles ink purchased from ANP, the Ag electrode is formed well. So we use this Ag ink and the device is fabricated with following structure: ITO/ZnO (40 nm)/PFN-P1 (2 mg/ml)/PDY-132 (80 nm)/V_2O_5 (1:200 vol. ratio)/Ag printing.

The J-V-L and EQE-J characteristics of all solution-processed PLED is shown in Figure 4.24. And the inset in Figure 4.24(b) shows the normalized EL spectrum at 51 mA/cm^2. The operating voltage is much higher than the PLEDs with vacuum-evaporated Ag cathode. The maximum EQE is 0.0056%; this value is also very low. The normalized EL spectrum is similar with the devices with vacuum-evaporated Ag cathode.

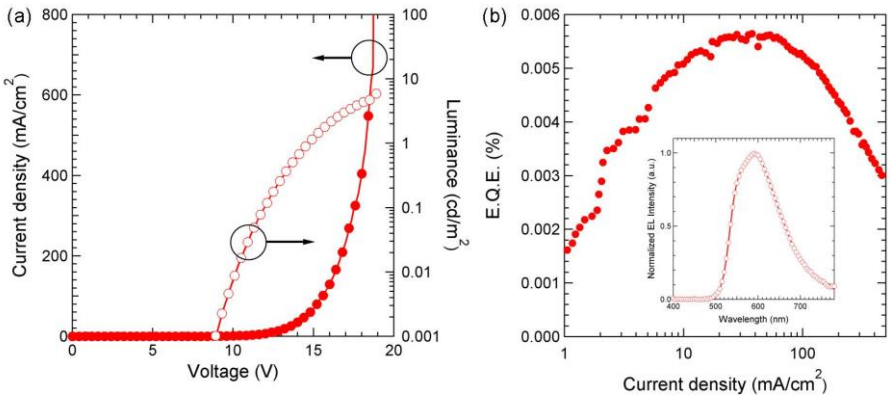

Figure 4.24 (a) J-V-L and (b) EQE-J characteristics of all solution-processed PLED with a inverted device structure. The inset in (b) shows The normalized EL spectrum at the current density (J = 51 mA/cm^2) of this device.

Chapter 5. Conclusion

In this thesis, high-performance solution-processed polymer light-emitting diodes have been studied in the view point of fabrication process and device structure. We developed and demonstrated all solution-processed polymer light-emitting diodes with ink-jet printed Ag electrode.

First, spin-coated KBH_4 doped 3TPYMB layer was introduced in PLEDs as n-type doped ETL and compared to PLEDs without this layer. The red, yellow, green and blue PLEDs with this n-doped ETL showed outstanding device performances than the devices without this layer. We measured the UPS spectra of the non-doped 3TPYMB and KBH_4 doped 3TPYMB films to understand the role of KBH_4 in improving the electron injection and transport properties. This result show that vacuum level was shifted by the dipole moment, and thus, electron injection can be enhanced at the interface. As the result, the device performances of PLEDs with n-doped ETL were improved. Furthermore, two conjugated polyelectrolyte materials, PEO and PFN-P1, were introduced in fabrication of high-performance PLEDs. These devices also show better performance. In case of PLEDs with KBH_4 doped 3TPYMB layer and PFN-P1 layer, the devices show good performance with Liq/Al bilayer cathode as well as with Ag electrode. Based on this result, we fabricate all solution-processed PLEDs using ink-jet printed Ag electrode. However, those layers are dissolved by Ag solvent and device fabrication is impossible. To solve this problem, ink-jet printed Ag is applied on PDMS and it is

transplanted onto pre-fabricated PLEDs. The device was working, but device performances were poor because the adhesion between pre-fabricated PLED and printed Ag electrode on PDMS was bad.

Second, we fabricated solution-processed PLEDs with an inverted device structure. For improving electron injection, self-assembled monolayer was applied to ZnO layer. Because the electron injection barrier between ZnO layer and EML was so high (~1.3 eV), device performances of the PLED with SAM was still low. To solve this problem, PFN-P1 layer which was successfully working in PLEDs with a conventional device structure was introduced in the PLEDs with an inverted device structure. The devices with PFN-P1 layer showed much higher device performances compared to PLEDs with SAM. Furthermore, several solution-processed hole injection layers were introduced in PLEDs with this PFN-P1 layer; FSO-100 doped PEDOT:PSS, MoO_3 nanoparticles and sol-gel V_2O_5. PLEDs with sol-gel V_2O_5 showed best performance above all. Finally, we fabricated all solution-processed inverted PLEDs with sol-gel V_2O_5 and direct ink-jet printed Ag. This device showed worse device performances compared to PLEDs with vacuum-evaporated Ag cathode, but better device performances compared to all solution-processed PLEDs with a conventional device structure.

We believe that the device design and the fabrication method can be utilized to realize the high efficient all solution-processed OLEDs.

Bibliography

[1] M. Pope, H. P. Kallmann and P. Magnante, *The Journal of Chemical Physics* **38**, 2042 (1963).

[2] P. S. Vincett, W. A. Barlow, R. A. Hann and G. G. Roberts, *Thin Solid Films* **94**, 171 (1982).

[3] C. W. Tang and S. A. VanSlyke, *Applied Physics Letters* **51**, 913 (1987).

[4] C. W. Tang, S. A. VanSlyke and C. H. Chen, *Journal of Applied Physics* **65**, 3610 (1989).

[5] J. H. Burroughes, D. D. C. Bradley, A. R. Brown, R. N. Marks, K. Mackay, R. H. Friend, P. L. Burn and A. B. Holmes, *Nature* **347**, 539 (1990).

[6] M. A. Baldo, D. F. O'Brien, Y. You, A. Shoustikov, S. Sibley, M. E. Thompson and S. R. Forrest, *Nature* **395**, 151 (1998).

[7] M. A. Baldo, S. Lamansky, P. E. Burrows, M. E. Thompson and S. R. Forrest, *Applied Physics Letters* **75**, 4 (1999).

[8] Y. Kawamura, K. Goushi, J. Brooks, J. J. Brown, H. Sasabe and C. Adachi, *Applied Physics Letters* **86**, 071104 (2005).

[9] S. Moller and S. R. Forrest, *Journal of Applied Physics* **91**, 3324 (2002).

[10] Y.-H. Cheng, J.-L. Wu, C.-H. Cheng, K.-C. Syao and M.-C. M. Lee, *Applied Physics Letters* **90**, 091102 (2007).

[11] R. Bathelt, D. Buchhauser, C. Gärditz, R. Paetzold and P. Wellmann, *Organic Electronics* **8**, 293 (2007).

[12] T. Tsutsui, M. Yahiro, H. Yokogawa, K. Kawano and M. Yokoyama, *Advanced Materials* **13**, 1149 (2001).

[13] Y. Sun and S. R. Forrest, *Nat Photon* **2**, 483 (2008).

[14] F. Huang, Y.-J. Cheng, Y. Zhang, M. S. Liu and A. K. Y. Jen, *Journal of Materials Chemistry* **18**, 4495 (2008).

[15] F. Huang, H. Wu and Y. Cao, *Chemical Society Reviews* **39**, 2500 (2010).

[16] J. S. Kim, P. K. H. Ho, C. E. Murphy, N. Baynes and R. H. Friend, *Advanced Materials* **14**, 206 (2002).

[17] J. Meyer, R. Khalandovsky, P. Görrn and A. Kahn, *Advanced Materials* **23**, 70 (2011).

[18] K. Zilberberg, S. Trost, J. Meyer, A. Kahn, A. Behrendt, D. Lützenkirchen-Hecht, R. Frahm and T. Riedl, *Advanced Functional Materials* **21**, 4776 (2011).

[19] N. Ozer and C. M. Lampert, *Thin Solid Films* **349**, 205 (1999).

[20] J. Meyer, S. Hamwi, T. Bulow, H. H. Johannes, T. Riedl and W. Kowalsky, *Applied Physics Letters* **91**, 113506 (2007).

[21] T. Shizuo, N. Koji and T. Yasunori, *Journal of Physics D: Applied Physics* **29**, 2750 (1996).

[22] H. You, Y. Dai, Z. Zhang and D. Ma, *Journal of Applied Physics* **101**, 026105 (2007).

[23] T. M. Brown, R. H. Friend, I. S. Millard, D. J. Lacey, J. H. Burroughes and F. Cacialli, *Applied Physics Letters* **79**, 174 (2001).

[24] L. S. Hung, C. W. Tang and M. G. Mason, *Applied Physics Letters* **70**, 152 (1997).

[25] H. J. Bolink, E. Coronado, J. Orozco and M. Sessolo, *Advanced Materials* **21**, 79 (2009).

[26] F. Huang, H. Wu, J. Peng, W. Yang and Y. Cao, *Current Organic Chemistry* **11**, 1207 (2007).

[27] C. Pacholski, A. Kornowski and H. Weller, *Angewandte Chemie International Edition* **41**, 1188 (2002).

[28] J. Y. Kim, S. Noh, D. Lee, P. K. Nayak, Y. Hong and C. Lee, *Journal of Nanoscience and Nanotechnology* **11**, 5995 (2011).

[29] K. Cho, S. W. Cho, P. E. Jeon, H. Lee, C.-N. Whang, K. Jeong, S. J. Kang and Y. Yi, *Synthetic Metals* **158**, 984 (2008).

[30] P.-C. Kao, J.-H. Lin, J.-Y. Wang, C.-H. Yang and S.-H. Chen, *Journal of Applied Physics* **109**, 094505 (2011).

[31] G. Parthasarathy, C. Shen, A. Kahn and S. R. Forrest, *Journal of Applied Physics* **89**, 4986 (2001).

[32] S. Watanabe, N. Ide and J. Kido, *Japanese Journal of Applied Physics* **46**, 1186 (2007).

[33] M. Junwei, X. Y. Jiang, L. Zhang, C. Jin, Z. Xiaowen and Z. L. Zhang, *Semiconductor Science and Technology* **24**, 035009 (2009).

[34] J. Huang, G. Li, E. Wu, Q. Xu and Y. Yang, *Advanced Materials* **18**, 114 (2006).

[35] K. S. Yook, S. O. Jeon, S.-Y. Min, J. Y. Lee, H.-J. Yang, T. Noh, S.-K. Kang and T.-W. Lee, *Advanced Functional Materials* **20**, 1797 (2010).

[36] K. S. Yook, S. O. Jeon, C. W. Joo, J. Y. Lee, T.-W. Lee, T. Noh, H.-J. Yang and S.-K. Kang, *Synthetic Metals* **159**, 1664 (2009).

[37] Q. Liu, D. Zhang, L. Duan, G. Zhang, L. Wang, Y. Cao and Y. Qiu, *Japanese Journal of Applied Physics* **48**, 080205 (2009).

[38] L. Duan, D. Zhang, Y. Li, G. Zhang and Y. Qiu, *Optics Express* **19**, A1265 (2011).

[39] D. Tanaka, T. Takeda, T. Chiba, S. Watanabe and J. Kido, *Chemistry Letters* **36**, 262 (2007).

[40] S. Khodabakhsh, D. Poplavskyy, S. Heutz, J. Nelson, D. D. C. Bradley, H. Murata and T. S. Jones, *Advanced Functional Materials* **14**, 1205 (2004).

[41] W. J. Zeng, H. B. Wu, C. Zhang, F. Huang, J. B. Peng, W. Yang and Y. Cao, *Advanced Materials* **19**, 810 (2007).

[42] R. Yang, H. Wu, Y. Cao and G. C. Bazan, *Journal of the American Chemical Society* **128**, 14422 (2006).

[43] J. H. Seo and T.-Q. Nguyen, *Journal of the American Chemical Society* **130**, 10042 (2008).

Publication

[1] International Journals

1. J. Y. Yun, **J. J. Yang**, Y. T. Hong, C. H. Lee, W. J. Song, Y.J. Sung, "Low driving voltage and long lifetime organic light-emitting diodes with molybdenum oxide (MoO_3) doped hole transport layer", *Journal of the Korean Physical Society* **53**, 1660 (2008).
2. S. U. Noh, **J. J. Yang**, S. H. Kim, C. H. Lee, "Investigation into the thermal annealing effect on the photovoltaic properties of organic solar cells based on CuPc/C_{60} heterojunctions", *Journal of the Korean Physical Society* **53**, 1551 (2008).
3. **J. J. Yang**, C. K. Suman, C. H. Lee, "Effect of type-II quantum well of m-MTDATA /α-NPD on the performance of green organic light emitting diodes", *Microelectronics Journal* **40**, 63 (2009).
4. **Jungjin Yang**, C.K.Suman, Changhee Lee, "Tandem white organic light emitting diodes consisting of blue and red phosphorescent unit devices connected with a transparent Al:LiF/MoO_3 connecting layer", *Proc. of SPIE* **7415**, 74151X (2009).
5. C. K. Suman, **J. J. Yang**, C. H. Lee, "Temperature dependent transport properties in molybdenum oxide doped α-NPD", *Materials Science and Engineering B* **166**, 147 (2010).

6. **Jungjin Yang**, C. K. Suman, Changhee Lee, “Studies of electroluminescent characteristics of quantum well green organic light emitting diodes”, *Molecular Crystals and Liquid Crystals* **520**, 273 (2010).
7. **Jungjin Yang**, C.K.Suman, Joonyoup Kim, Won-Jun Song, Sanghyuk Wooh, Kookheon Char, Changhee Lee, “Fabrication of Transparent Al:LiF composite/MoO_3 interconnecting layers for tandem white organic light emitting devices”, *Journal of Nanoscience and Nanotechnology*, accepted (Aug, 2011)

[2] International Conferences

1. S. U. Noh, J. Y. Kim, **J. J. Yang**, S. H. Kim, and C. H. Lee, "Investigation into temperature dependence on the properties in CuPc-C_{60} photovoltaic cells", The 5th International Conference on Advanced Materials and Devices, Jeju, Korea, Dec. 12-14 (2007).
2. J. Y. Yun, **J. J. Yang**, W. J. Song, Y. J. Sung, and C. H. Lee, "Low driving voltage and long lifetime organic light-emitting diodes with molybdenum oxide(MoO_3) doped hole transport layer", The 5th International Conference on Advanced Materials and Devices, Jeju, Korea, Dec. 12-14 (2007).
3. C. H. Kim, **J. J. Yang**, C. H. Lee, H. Y. Oh and S. H. Lee, "Effect of a Hole Transport Layer on the Magnetic Field Effect of the Electroluminescence in Organic Light-Emitting Diodes", MRS Spring Meeting, San Francisco, USA, Mar. 24-28 (2008).
4. **J. J. Yang**, S. U. Noh and C. H. Lee, "Photovoltaic Properties of Organic Solar Cells with CuPc/C_{60} Heterojunctions and Transparent Top and Bottom Electrodes Under Light Illumination through Both Sides", MRS Spring Meeting, San Francisco, USA, Mar. 24-28 (2008).
5. C. K. Suman, **J. J. Yang**, H. D. Cho and C. H. Lee, "Studies on conduction mechanism of metal oxide doped organic semiconductor using impedance spectroscopy", ICEL-7, Dresden, Germany, Sep. 2-6 (2008).

6. **J. J. Yang**, H. D. Cho, S. U. Noh, Y. T. Hong and C. H. Lee, "Investigation of temperature dependence of the hole mobility in poly(3-hexylthiophene) thin film transistor", MRS Fall Meeting, Boston, USA, Dec. 1-5 (2008).
7. **J. J. Yang**, C. K. Suman, J. Y. Kim, W. J. Song, and C. H. Lee, "Tandem white organic light emitting diodes consisting of blue and red phosphorescent unit devices connected with a transparent Al:LiF/MoO_3 connecting layer", SPIE, San Diego, USA, Aug. 1-6 (2009).
8. **J. J. Yang**, C. K. Suman and C. H. Lee, "Studies of Electroluminescent Characteristics of Quantum Well Green Organic Light Emitting Diodes", KJF-ICOMEP, Jeju, Korea, Aug. 23-26 (2009).
9. **J. J. Yang**, C. K. Suman and C. H. Lee, "Tandem white organic light emitting diodes comprising of red, green, blue emission", IMID, Seoul, Korea, Oct. 12-16 (2009).
10. Hyunkoo Lee, **Jungjin Yang**, Hyuk Ahn, and Changhee Lee, "Improvement of power efficiency of phosphorescent white organic light-emitting diodes with p-doped hole transport layer", The 8th ICEL 2010, Michigan, USA, Oct. 17-21 (2010).
11. **Jungjin Yang**, Jae Joon Jo, Dong Ryeol Whang, Youngmin You, Soo Young Park, and Changhee Lee, "A highly efficient electrophosphorescent device with novel blue phosphorescent Ir(III) complex", Pacifichem 2010, Hawaii, USA, Dec. 15-20 (2010).

12. **Jungjin Yang**, C.K. Suman, Joonyoup Kim, Won-Jun Song, and Changhee Lee, “Transparent Interconnecting Layer of Al:LiF Composite/MoO_3 for Tandem White Organic Light Emitting Devices”, The 22nd ICME&D, Pohang, Korea, May. 19-20 (2011).
13. Hyuk Ahn, Hyunkoo Lee, **Jungjin Yang**, and Changhee Lee, “Highly efficient electron-injection layer of LiF/Yb bilayer for top-emitting OLEDs”, 50th SID International Symposium, Seminar & Exhibition, Boston, USA, June 3-8 (2012).
14. SuYeon Park, Hyunkoo Lee, **Jungjin Yang** and Changhee Lee, “Simulation of CRI and CCT for white OLEDs consisting of three different colors”, ICSM 2012, Atlanta, USA, July 8-13 (2012).

[3] Domestic Conferences

1. 양정진, 노승욱, 이창희, 효율적인 2 파장 백색 유기 발광 소자 연구 (Investigation of efficient white organic light emitting devices with two primary colors), The Optical Society of Korea Annual Meeting, Seoul, Korea, Feb. 14-15 (2008).

초 록

유기 발광 다이오드는 평판 디스플레이와 조명에 있어 큰 가능성을 가지고 있는 기술로 주목을 받고 있다. 유기 발광 다이오드는 진공 증착과 용액 공정을 통해서 제작이 가능한데, 용액 공정을 사용할 경우 빠른 생산 속도와 저 비용 공정의 측면에서 장점이 있다. 이와 관련된 많은 연구가 진행되었고, 또한 많은 성과가 있었다. 하지만 그럼에도 불구하고 전 용액 공정 유기 발광 다이오드 제작에 대한 시도는 거의 없었다. 본 논문에서는 용액 공정을 이용한 고분자 발광 다이오드의 제작 및 소자의 성능을 연구하였고, 마지막으로 전 용액 공정 고분자 발광 다이오드를 제작하였다.

정구조 소자에서 용액 공정을 이용한 KBH_4 가 도핑된 3TPYMB 를 n-도핑된 전자 수송층으로 사용하여 소자를 제작하였고, 좋은 소자 특성을 나타냈다. 또한 두 가지의 공액 고분자 전해질 (PEO, PFN-P1)을 사용하여 소자를 제작하였고, 이 역시 좋은 소자 특성을 나타냈다. 이 중에서도 KBH_4 가 도핑된 3TPYMB 와 PFN-P1 을 사용한 소자의 경우, Liq/Al 이중 박막 음극을 사용했을 때 뿐 아니라 은 단일 음극을 사용했을 때에도 좋은 소자 특성을 보였다. 이를 바탕으로 잉크젯 프린팅을 이용한 은 전극을 사용하여 전 용액 공정 고분자 발광 다이오드 제작을 해봤지만, 은 잉크의 용매에 박막이 녹아서 소자 제작이 불가능했다. 이를 해결하기

위해서 PDMS 에 은을 프린팅하여 전극을 형성한 후 미리 제작한 소자에 이식하는 방법을 사용하여 전 용액 공정 고분자 발광 다이오드를 제작하였다.

나아가 역구조 소자에 대한 연구도 진행하였다. 전자의 주입을 향상시키기 위하여 자가조립 단분자막을 이용해서 ZnO 박막 위에 계면처리를 하였다. 하지만 그 효과가 작아서 정구조 소자에서 사용했던 PFN-P1 박막을 역구조 고분자 발광 다이오드 제작에도 적용하였다. 그 후 정공 주입층에 용액 공정을 도입하기 위하여 FSO-100 을 첨가한 PEDOT:PSS, MoO_3 나노입자층 그리고 sol-gel V_2O_5 을 사용하여 소자를 제작하였고, sol-gel V_2O_5 을 사용하였을 때 가장 좋은 성능을 보임을 확인 하였다. 마지막으로 sol-gel V_2O_5 와 은 잉크젯 프린팅을 이용하여 전 용액 공정 고분자 발광 다이오드를 제작하였다. 본 논문에서 개발된 공정 방법들과 소자 구조들은 미래에 더 좋은 효율을 갖는 전 용액 공정 유기 발광 다이오드를 제작하는데 도움이 될 것으로 생각된다.

주요어: 용액 공정, 고분자 발광 다이오드, n-도핑, 공액 고분자 전해질, 잉크젯 프린팅

학 번: 2007-21014